EXPERIMENTAL INVESTIGATION OF TWO-PHASE INSTABILITY IN NATURAL CIRCULATION WITH DIRECT TRANSIENT LOCAL MEASUREMENT

BY

TAIYANG ZHANG

THESIS

Submitted in partial fulfillment of the requirements
for the degree of Master of Science in Nuclear, Plasma, and Radiological Engineering
in the Graduate College of the
University of Illinois at Urbana-Champaign, 2019

Urbana, Illinois

Master's Committee:

Assistant Professor Caleb S. Brooks
Professor Rizwan Uddin

ABSTRACT

Nuclear reactor systems can be susceptible to thermal hydraulic instability under specific circumstances. Proper handling of the stability problem under natural circulation is critical for the reactor safety and operation under important conditions such as the start-up transient of natural circulation cooled boiling water reactors. This experimental research focuses on the two-phase instability under low system pressure (1 - 10 atm) in a natural circulation loop where an adiabatic riser is present above the heated section. Direct transient local measurement of two-phase flow is performed at multiple axial locations along the flow channel with thermocouples and conductivity probes traversed by customized high-precision mechanisms. Periodic oscillation is captured when the vapor quality at the test section exit is close to zero. A post-processing method is proposed to extract the oscillation cycles and reconstruct the instability behavior in one representative period. An averaging operation over multiple oscillation cycles is performed to reduce the random errors. Cyclic phenomena are clearly demonstrated by the post-processed data, and rapid void fraction change induced by the flashing is observed to be significant in the driving mechanism for low pressure oscillations. Parametric effects of inlet subcooling, heat flux, inlet flow restriction and system pressure are studied within the experiment range, and qualitative results are explained and compared with existing literature. The ratio between the oscillation period and the travelling time of the fluid particle is compared with the theoretical value for the density wave oscillation. The conditions captured form a new dataset containing directly-measured transient multi-dimensional two-phase data along the flow channel for natural circulation under density wave oscillations. The generated dataset is valuable for the validation of safety analysis codes and CFD codes in the simulation of natural circulation phenomena and dynamic two-phase flow.

ACKNOWLEDGEMENTS

This material is partially based upon work supported by the Department of Energy under award number DE-NE0008573.

The author would like to express gratitude to Prof. Caleb S. Brooks for his consistent support, patient guidance and inspiring advises on this project. Sincere thanks are given to my colleague Maciej Skrzypek for his important collaboration in performing the experiment. Special credit is also given to my colleague Zhiee Jhia Ooi who provides the steady-state test data, instructs the operation of the facility and shares important experience as an experimentalist. The author highly appreciates the chance of carrying out this promising project and values all the support he gets in the progress.

Appreciation is expressed here to Prof. Rizwan Uddin who generously spends his precious time in reviewing and critiquing this thesis.

TABLE OF CONTENTS

NOMENCLATURE v

CHAPTER 1: INTRODUCTION 1

1.1 General Background 1

1.2 Literature Review 3

1.3 Objectives and Outline 8

CHAPTER 2: METHOD 9

2.1 Facility and Instrumentations 9

2.2 Experiment Procedure and Test Matrix 12

2.3 Post-processing Method 15

CHAPTER 3: RESULT AND DISCUSSION 22

3.1 Stability Maps 22

3.2 Example Data and Cyclic Phenomena 24

3.3 Parametric Effects 31

3.4 Oscillation Period and Fluid Particles' Residence Time 34

CHAPTER 4: CONCLUSIONS AND FUTURE WORK 39

4.1 Conclusions 39

4.2 Future Work 40

REFERENCES 42

APPENDIX A: UNCERTAINTY 47

A.1 General Procedure 47

A.2 Instrumentational Uncertainty 47

A.3 Overall Uncertainty 49

NOMENCLATURE

D_h	hydraulic diameter [m]
i	specific enthalpy [J/kg]
K_{loss}	inlet pressure loss coefficient [-]
N_{pch}	phase change number (Zuber number) [-]
N_{sub}	subcooling number [-]
P	pressure [Pa]
q	heat flux [W/m^2]
Q	total heating power [W]
r	radial location [m]
R_i	inner diameter of the annulus channel [m]
R_o	outer diameter of the annulus channel [m]
R^*	dimensionless radial location [-]
x	vapor quality [-]
t	time [s]
T	fluid temperature [°C]
v	inlet flow velocity [m/s]
W	mass flow rate [kg/s]
z	axial location [m]

Greek

α	void fraction [-]
ΔP	differential pressure [Pa]
Δt	time-window width [s]
ρ	density [kg/m^3]

Subscripts

1~5	index of the measurement port
ch	chimney
f	liquid phase
g	gas phase
m	two-phase mixture
in	test section inlet
sat	saturation
sub	subcooling

Bracket

< >	area-averaged value

CHAPTER 1: INTRODUCTION

1.1 General Background

Two-phase flow systems can be susceptible to various flow instabilities which lead to undesirable dynamic behaviors possibly causing mechanical vibrations, difficulty in controlling and even failure of components [1]. Historical events in nuclear reactor systems indicate that the presence of thermal-hydraulic instabilities can lead to complex and challenging conditions. One such example is the March 9, 1988 recirculation pump trip at the LaSalle Unit-2 reactor [2]. Instability under natural circulation following an unexpected recirculation pump trip caused the core power to oscillate with a peak-to-peak value around 25% rated power every 2 to 3 seconds, which eventually triggered the automatic scram 7 minutes after recirculation pump trip. The review of this event found that at the time of reactor scram, the magnitude of power oscillation was at least 100% peak-to-peak, which was unexpected based on previous operating experience. Instability was also observed in the restart of the Washington Nuclear Power Unit-2 on August 15, 1992 [3]. During the closing of one of the flow control valves in preparation for increasing the recirculation pump's speed, oscillations were observed on the power range monitors and the operators manually scrammed the reactor at once. Post-event review indicated that 2-second-period oscillations had grown to a peak-to-peak amplitude of 25% rated power within one minute and became self-sustained for an additional minute before the scram. The primary cause of the oscillation was found to be the very skewed core power distributions that resulted partially from the rod patterns with unbalanced flow characteristics.

The susceptibility of nuclear reactor systems to thermal hydraulic instability has demanded the attention of many of the pioneers in field of nuclear reactor safety [1, 4-8] and instability phenomena in two-phase flow are widely reported in literature. A general review has been

performed by Boure et al. [1] in which multiple types of instabilities have been summarized and classified based on their driving mechanisms. The onset of some instabilities, such as the famous Ledinegg instability, can be predicted by steady-state laws and therefore are classified as static instabilities. On the other side, dynamic instabilities such as the density wave oscillations, governed by the system dynamics involving the propagation of disturbances, intrinsically need to be predicted using more complicated dynamic governing equations. Boure et al. also point out that several elementary mechanisms can exist simultaneously, interact with each other and cause the compound instabilities. The diversity and complexity of the thermal-hydraulic instability justify the consistent effort of previous researchers and further emphasize the importance of a comprehensive understanding of the instability phenomena in nuclear reactor systems.

As reviewed by Nayak and Vijayan [9], while most two-phase instabilities are observed in both forced convection and natural circulation systems, the latter has a higher chance of experiencing instabilities due to the strong coupling between the flow rate and driving force. Past experiments [10-11] find that self-sustainable flow oscillations with large magnitude and low frequency can happen in natural circulation at low pressure, which may cause significant challenges during the startup of natural circulation boiling water reactors (NCBWRs). Tests on the natural-circulation-cooled Dodewaard reactor further confirm that the reactor can experience instability at low pressure and low power [12]. Experiments have been a critical piece to further the understanding of thermal-hydraulic instability in two-phase naturel circulation systems and have been performed by numerous researchers resulting in data of different forms and resolutions. The focus of this thesis is on instability under natural circulation at low system pressure and therefore several important experiments and datasets under these conditions are reviewed.

1.2 Literature Review

As a brief summary, Table 1 lists several existing experiments on the instability under two-phase natural circulation. Despite the variety in detailed loop configurations, a common geometry characteristic of these loops is the unheated section with considerable elevation or volume above the heated section. The unheated riser, present commonly in these test facilities and their prototype natural circulation systems, increases the difference in gravitational pressure drops between the cold leg and the hot leg, which provides higher driving force for the natural circulation. One the other hand, as argued by Fukuda et al. [13], because of the consequently enhanced feedback between the flow rate and the driving force, the presence of unheated riser plays a dominant role in inducing the instability at near-zero vapor quality conditions, i.e., the Type-I density wave oscillation named in their research. Experimental investigations [10-11] further point out that the unheated section can introduce phase change with steep jump in the void fraction and therefore in the driving force, e.g. the rapid condensation in the large unheated section, and the sudden vapor generation due to the loss of hydrostatic pressure along the vertical adiabatic chimney. Similar to the research listed in Table 1, this thesis focuses on the instability phenomena in a natural circulation loop where an adiabatic riser is installed above the heated section. The operational conditions are chosen under low vapor quality and low system pressure (1 – 10 atm).

Existing experiments present datasets with different resolutions and forms depending on their main objectives and available instrumentations as shown in Table 1. One of the main objectives of this thesis is to collect data with improved quality, so a review for the existing datasets focusing on the data form and measurement strategy is performed.

Table 1: Existing experiments and datasets

Research	Loop Configuration	Directly Measured Parameters	Two-phase Measurement	Data form
Aritomi et al., 1992 [10]	Two parallel heated channels below a large separator tank	Flow rate, pressure, and temperature	N/A	Spatially 1D temporal signals, and stability maps
Furuya et al., 1995 [11]	Two 1.7m parallel heated channels below a 5.7m adiabatic chimney upstream a separator tank (SIRIUS-N)	Flow rate, pressure, and temperature	Void fraction estimated by the mixture momentum equation	Spatially 1D temporal signals, and stability maps
Kim and Lee, 2000 [14]	A 1.5m heated channel below a 1.0m unheated channel	Flow rate, pressure, and temperature	Void fraction estimated by the pressure drop	Spatially 1D temporal signals and stability maps
Manera and van der Hagen, 2003 [15]	Four 1.95m parallel heated channels below a 3m adiabatic riser (CIRCUS)	Flow rate, pressure, temperature, and void fraction	Wire-mesh sensors, gamma-transmission, and conductivity needle probes	Spatially 1D temporal signals, local void fraction by wire-mesh sensors, and stability maps
Marcel et al., 2009 [16]	Four 1.95m parallel heated channels below a 3m adiabatic riser (CIRCUS)	Flow rate, pressure, temperature, and void fraction	Conductivity needle probes, and capacitance-based sensors	Spatially 1D temporal signals, and stability maps
Dixit et al., 2013 [17]	A scaled model facility for the integral modular water reactor (IMR)	Flow rate, pressure, temperature, and void fraction	Impedance probes	Spatially 1D temporal signals, and stability maps
Cloppenborg et al., 2015 [18]	An inclined section heated by steam condensation followed by a 7m vertical riser (GENEVA)	Flow rate, pressure, temperature, and void fraction	Triaxial conductivity probes	Spatially 1D temporal signals, local void fraction at two or three radial locations
Shi et al., 2015 [19]	A scaled model facility for the small modular water reactor (SMR) NMR-50	Flow rate, pressure, temperature and void fraction	Impedance probes	Spatially 1D temporal signals, and stability maps
Wang et al., 2018 [20]	A 1.6m heated channel below a 3m unheated riser.	Flow rate, pressure, and temperature	N/A	Spatially 1D temporal signals

The stability map is a common way to concisely exhibit the stability behavior of two-phase loops. Quasi-steady operational conditions are uniquely represented by points on the maps with marked stability. Research on the general characteristics of instability phenomena under natural circulation can exhibit the parametric effects clearly with stability maps [10, 14]. Moreover, for experiments on scaled facilities, stability tests covering large operational ranges are often organized as stability maps in order to instruct the prototype reactors' operation. Furuya et al. [11, 21] report the stability maps for the SIRIUS-N facility designed based on the scaling analysis of typical natural circulation boiling water reactors. On their stability maps, operational conditions are represented by the heat flux and the non-dimensional subcooling number. For experiments on the CIRCUS facility, a full-height scaled water loop of the Dodewaard reactor, Manera and van der Hagen [15] utilize dimensional subcooling-power planes to construct stability maps, out of the consideration for unambiguously presenting and directly predicting the operation points. A similar stability map is also used to experimentally validate the analytical stability boundaries obtained from a lumped Homogeneous Equilibrium Model by Marcel et al. [16]. The stability map for the Purdue's IMR instability test facility is constructed on the power-rate versus the non-dimensional subcooling number plane by Dixit et al. [17, 22]. Experiments on the NMR test facility are organized on a fully non-dimensional Zuber number-subcooling number stability map, which is used to determine the NMR-50's stability boundary by Shi et al. [19, 23]. Non-dimensional stability map is also drawn for the tests performed on the Dodewaard reactor to investigate the reactor's stability [24]. These stability maps are highly reduced data, whose main function is to concisely indicate the stability boundaries and to instruct the prototype reactors' operation.

Another common form of data is one-dimensional transient signals measured along natural circulation loops. Because these signals are identical or very close to the raw data directly

monitored in the experiments, their resolutions vary with available instrumentations. The SIRIUS-N facility records temperature, pressure, and flow rate signals simultaneously from direct measurement, and estimates void fraction based on the one-dimensional mixture momentum equation [21]. Two types of oscillation waveforms are recorded, and the flashing in the chimney is concluded to be the driving mechanism. On the other hand, the CIRCUS facility measures all these signals, and the void fraction evolution in the adiabatic riser is directly measured by a wire mesh sensor, advanced needle-probes and the Gamma-transmission [15]. Two oscillation waveforms are related to different phenomena patterns, and a phenomenological classification is proposed. While the data reported by these two studies are collected after stationary oscillations are reached, Dixit et al. [25] and Shi et al. [26] also report the signals during the startup transient with direct two-phase measurement. The one-dimensional data presented in these literatures simply keeps the major information recorded in experiments, which comprehensively exhibits the temporal waveforms under the operation conditions. However, it is also worthwhile to notice that these signals are usually one-time measured due to the intrinsically transient nature of instability phenomena, so their uncertainties caused by the random error cannot be estimated directly from a simple averaging procedure. These one-dimensional transient signals reveal detailed system behaviors for understanding instability phenomena.

Multi-dimensional measurement of transient two-phase natural circulation is rarely reported in literature. Non-intrusive methods such as radiation attenuation methods and the impedance sensors usually require proper tomography techniques to reconstruct the multi-dimensional two-phase structure [27-29], and their application in the transient local measurement on two-phase natural circulation loop is rare. Instrumentations capable of direct local measurement such as conductivity probes [15-16, 18, 30] and thermocouples [11, 15-19] often work with fixed

measurement points and give representative bulk values. On the GENEVA facility, Cloppenborg et al. [18] install up to three fixed conductivity probes with different radial locations at each axial measurement position. In their instability experiment using total 16 probes at 9 axial locations, the radial resolution for the local void fraction distribution is improved to up to 2 points including one at the center of the circular channel. The wire mesh sensor, which is specially designed to measure the two-phase parameters' transient distribution across the flow channel, has been used by Manera et al. [31] for the three-dimensional reconstruction of transient upward flashing flow, but may lead to large flow disturbances downstream [32]. In their research on the CIRCUS facility [15, 31], one double-layer wire mesh sensor is installed only near the outlet of the test section to limit this disturbance on the other measurements, and the void fraction and temperature upstream are measured by advanced needle-probes positioned at the centers of the channel. Another attempt to collect multi-dimensional data in natural circulation flow is performed by Ooi et al. [33] using conductivity probes and thermocouples mounted on traversing mechanisms. In Ooi et al.'s experiment, measurement points scan across the flow area, and the steady-state natural circulation flow is directly measured, including local two-phase parameters. While this method is suitable for steady-state conditions because of their time-independent nature, its applicability for transient cases still needs to be examined.

Periodicity of the oscillation provides the chance to improve the data's precision and resolution. Measuring a periodic parameter for multiple periods is equivalent to repeated sampling, which allows the estimation of random errors by a statistical averaging procedure. A practice reflecting this idea is reported in Manera et al.'s [31] reconstruction of the flow pattern for transient flashing flow. An averaging procedure over multiple oscillation periods, named as the ensemble average, is performed on the wire-mesh sensor signals to obtain statistically accurate velocity and

the void fraction. The outputted representative void fraction behavior is observably smoother than the inputted one-time measured signals [34]. Furthermore, the periodicity also allows signals to be recorded non-simultaneously, because instead of the absolute time, a representative time in one period can be used to express the periodic behavior. The traversing mechanisms with conductivity probes and thermocouples are applicable if signals from different radial locations can be synchronized to the common representative time by post-processing. The periodic oscillations can thus be recorded multi-dimensionally by a limited number of instrumentations and with a better precision than one-time-measured signals, which provides promising data valuable for revealing the instability details and serving for code validation.

1.3 Objectives and Outline

The objective of thesis is to reconstruct the periodic oscillations induced by instability in natural circulation at low system pressure as multi-dimensional transient data and to analyze the instability's basic characteristics.

To achieve these goals, experiments are performed on a two-phase water loop. Traversing mechanisms with conductivity probes and thermocouples are used for direct local measurement. Post-processing is performed to synchronize signals and average the data over multiple oscillation cycles. Cyclic phenomena in the oscillations are analyzed in detail. Qualitative parametric effects are summarized and compared with other literature. The motion of two-phase mixture is traced based on the continuity equation, and the relation between the oscillation period and the travelling time of particles are discussed. The current research is novel in its measurement of local two-phase flow at multiple axial locations under periodic conditions, which first expands the existing datasets to include multi-dimensional data for transient conditions.

CHAPTER 2: METHOD

Details of the experiment and the post-processing method is described in this chapter. Experiments under two-phase natural circulation are performed at low system pressure on the same facility used by Ooi et al. [33]. Conditions with periodic oscillations induced by instability are recorded with direct local measurement through thermocouples and conductivity probes mounted on traversing mechanisms. A specific procedure is used for the online adjustment of the radial measurement locations, and an associated post-processing method is developed to extract and synchronize all oscillation cycles onto one representative period.

2.1 Facility and Instrumentations

As a reference, a complete overview of this experimental facility and its operation under steady-state natural circulation can be found in Ooi et al. [33]. For the current experiment, the facility's important features and its operation under transient conditions are summarized here.

The experimental facility is a closed system consisting of a water loop connected to a pressurizing tank (Fig.1). The test section (Component A) is a concentric annular flow channel about 5 m high, whose inner and outer diameters are 19.05 mm and 38.10 mm, respectively. The test section is mainly composed of a heated section and an adiabatic chimney, where a 3000 mm cartridge heater followed by a 1990 mm unheated rod serves as its inner rod. A short unheated annular section of 197mm long is present between the test section inlet and the beginning of the heated section. A four-pass shell-and-tube heat exchanger (Component B) is installed on the top of the facility to condense any vapor generated from the test section and to maintain the required subcooling for downstream flow. During natural circulation experiments, the pump isolation valve (Component H) is closed while the bypass ball valve (Component C) is fully open, so the pump

bypass line is the only return line for the cold water. The globe valve (Component E) upstream the test section inlet serves as a controller of the inlet flow restriction, whose local friction loss coefficient K_{loss} is determined experimentally in single-phase forced convection tests and correlated with the rotation of the valve handwheel. A pressurizing tank pressurized by nitrogen (Component I) is connected to the loop to provide a compressible space for the system and to maintain the required inlet pressure level.

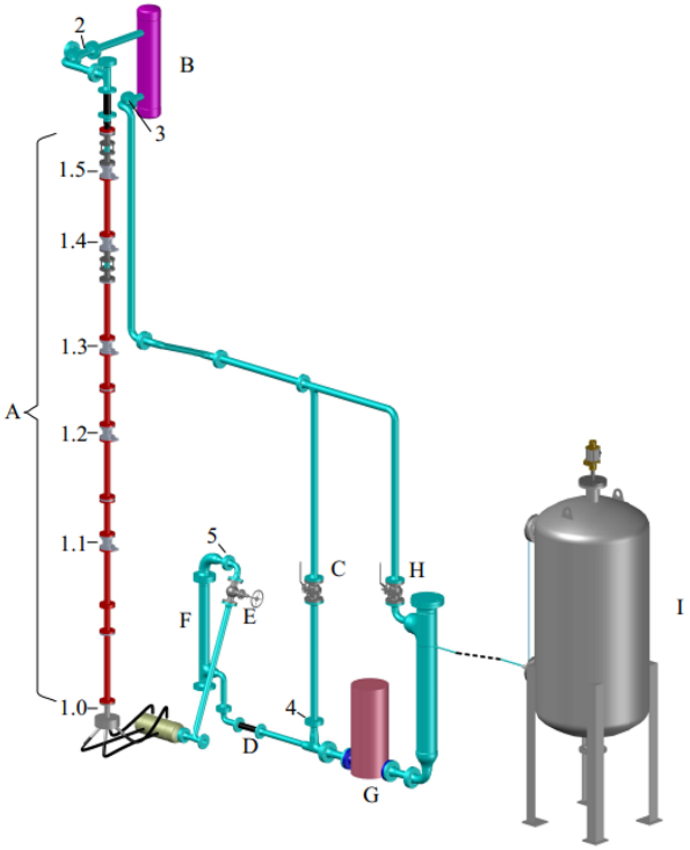

Component	Description
A	Test section
B	Condenser
C	Bypass ball valve (fully open)
D	Flowmeter
E	Globe valve
F	Preheater (off)
G	Pump (off)
H	Pump isolation valve (closed)
I	Pressurizing tank

Measurement Location	Description
1.0	Test section inlet
1.1 - 1.5	Port 1 - Port 5
2	Condenser inlet
3	Condenser outlet
4	Return line outlet
5	Preheater outlet

Figure 1: The experimental facility. Inside the parentheses are the working states of components when the facility is in natural circulation mode**.**

Deionized water is the working fluid of the loop. For the proper working of conductivity probes and the magnetic flow meter, the conductivity of water is maintained at around 40 μS by adding about 10 mL of ammonium hydroxide and morpholine solution, which also controls the

water quality. Compressed nitrogen only occupies the top quarter of the tank volume. The tank is connected to the loop through a long surge line to limit the diffusion of nitrogen to the degassed loop system. The water level in the tank is measured with a tubular level indicator and maintained at nearly equal level for different test conditions. Different from the steady-state situation, under transient conditions the compressible volume in the pressurizing tank influences the system dynamics by introducing the feedback effect between the system pressure and the void fraction in the loop [15], so controlling the compressible volume is important for the parametric study of instability phenomena.

Instrumentations are mounted along the loop at the locations labeled by the numbers in Fig.1. Inlet volumetric flow rate is measured by a magnetic flow meter (Component D). Power to the cartridge heater is controlled by a solid-state unit, and the temperature of the heating rod is also monitored with internal K-type thermocouples buried below the rod surface. Absolute system pressure is measured at the test section inlet by a gauge pressure transmitter, and differential pressures between the inlet and other nine locations are also recorded by a differential pressure transmitter. Ungrounded T-type thermocouples are mounted at ten locations for fluid temperature measurement. The five instrumentation ports along the test section are equipped with four-sensor conductivity probes [30] to capture local two-phase parameters. The distances from the inlet of test section to the five ports are z/D_h = 79.3, 128.3, 167.0, 214.7, 246.7. It is worth noting that the Port 3 is at the outlet of the heated section.

For the five instrumentation ports on the test section, customized traversing mechanisms are installed to perform local measurement across the flow area. Each traversing mechanism is equipped with a thermocouple or a conductivity probe whose radial location is accurately controlled by a precision screw gauge with a resolution of 10 μm. Every instrumentation port has

two traversing mechanisms on which a thermocouple and a conductivity probe are positioned in two perpendicular angular directions. Angular symmetry is assumed for the flow and therefore the measurement covering multiple radial locations can represent the parameters' distributions on the flow area.

2.2 Experiment Procedure and Test Matrix

Degassing is performed before setting the test conditions. For degassing, the facility is operated in the forced-convection mode with the pump working, the isolation valve fully open, and the bypass ball valve partially closed. Water is heated with the preheater and the main cartridge heater to its saturation temperature in the test section, and the vapor is condensed in the condenser which causes the non-condensable gases to accumulate at the top of the facility. The trapped gas is eliminated frequently through vent lines. After degassing, the preheater and the pump are turned off, the pump isolation valve is closed, and the bypass ball valve is fully open. The facility is then operated in natural circulation mode as shown by the description in Fig.1.

Operation conditions are set based on the inlet absolute pressure P_{in}, the inlet subcooling $\Delta T_{sub,in}$, the heat flux q, and the inlet minor loss coefficient K_{loss}. These four parameters are controlled by the pressurizing tank, the condenser, the main heater, and the globe valve, respectively. Generally, under conditions exhibiting instability, the inlet pressure oscillates periodically with small magnitude compared with its averaged value, while the fluctuations in the inlet subcooling are small and comparable with the instrumentational uncertainty. Therefore, time-averaged values of inlet absolute pressure and inlet subcooling are used as nominal reference for the conditions, which is satisfactory enough for performing parametric analysis.

Before recording, sufficient time is spent to reach either steady states for stable conditions, or periodic oscillations for conditions showing instability. Real-time signals are monitored to ensure that conditions can remain longer than 30 minutes before recording, and the recorded data are further checked in post-processing. Oscillation waveforms are required to exhibit consistency and no monotonic trend in their periods, maxima and minima.

Data recording is performed in multiple measurement steps where the radial location is changed stepwise for all probes and thermocouples in the test section, Fig. 2. Non-dimensional radial location defined by $R^* = (r - R_i)/(R_o - R_i)$ is used to label the measurement location, where R_i and R_o are the inner and outer radii of the test section. In the current experiment, local measurement is performed at 11 locations R^* = 0.1, 0.15, 0.2, 0.3, 0.4, 0.5, 0.6, 0.7, 0.8, 0.85, 0.9. For the regions less than 0.95mm to the walls, i.e., $R^* < 0.1$ and $R^* > 0.9$, direct measurement is not performed due to the limitation in the size of conductivity probes and ungrounded thermocouples. Each measurement step lasts for more than ten oscillation periods and no less than 240 seconds. Signals from all instrumentations are always recorded simultaneously.

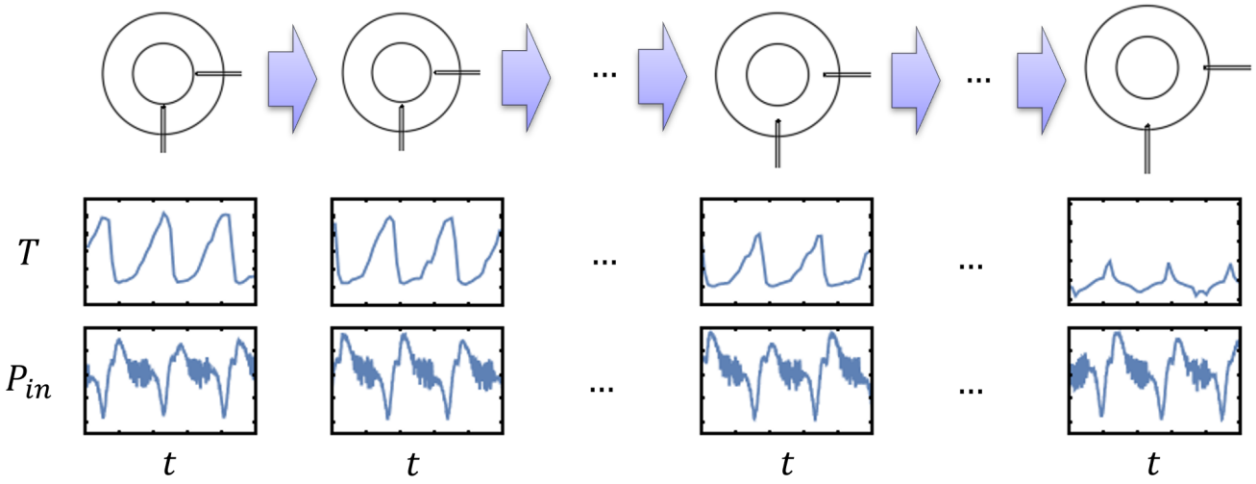

Figure 2: Stepwise adjustment of the radial locations for the local measurement. The first row shows the conceptual cross section views of the flow channel, while the two rows below exhibit typical signal patterns recorded in multiple measurement steps.

Two sets of tests are performed with the system pressure nearly equal to 190kPa and 500kPa respectively. All the periodic conditions are shown in the test matrix of Table 2. For either pressure level, one condition exhibiting obvious periodic oscillations is firstly identified when the measured local fluid temperature at the top of the test section shows that the flow changes from subcooled to saturated, which is marked by the bold parameter values in Table 2. A set of conditions are then achieved by changing either the inlet subcooling, the heat flux, or the inlet pressure loss coefficient and keeping other two parameters unchanged until the stability boundary is crossed. Thus, each non-bold number in Table 2 represents one condition with two bold parameter values at that pressure. For example, the non-bold value $T_{sub,in}$ = 13.2 ^{o}C in the second column represents a condition captured with P_{in} = 190kPa, $T_{sub,in}$ = 13.2 ^{o}C, q = 32.7 kW/m^2 and K_{loss} = 22.1.

Table 2: Test matrix. It is formed through common boundary conditions for each pressure given in bold. Every condition with a non-bold parameter has corresponding bold values for the other two parameters.

Inlet Pressure, P_{in} (kPa)	**190**	**500**
Number of Conditions	12	8
Inlet Subcooling, $T_{sub,in}$ (^{o}C)	13.2, 15.9, **18.4**, 20.7	15.3, **18.1**, 21.2, 25.3
Heat Flux, q (kW/m^2)	18.5, **32.7**, 45.4, 66.2, 100.8, 134.8	87.6, **134.8**, 178.8
K_{loss} (-)	**22.1**, 42.3, 86.6, 157.9	**22.1**, 42.3, 30.4

2.3 Post-processing Method

The recorded signals are post-processed to reconstruct the periodic oscillations as multi-dimensional transient data. The periodicity makes it possible to improve the data's precision by averaging over multiple periods and to reconstruct the system behavior by combining local signals measure at different time. The basic idea is to express the signals measured at different oscillation cycles to a common representative time. The representative time shall fall on a one-period-long interval and indicate the state of the system. This approach can then provide a mean oscillation behavior of the flow. To obtain this common time a parameter that is always recorded during the experiment can be chosen to represent the state of the system. If the oscillation cycles in this parameter can be extracted and aligned, directly applying the same operation to other simultaneously measured parameters will align the oscillation cycles in all the signals.

To achieve this alignment all the signals are first resampled to a common frequency. The aim of equalizing the sampling frequencies is to simplify the processing procedure, and the resampling frequency is chosen as 100Hz to provide satisfactory alignment resolution.

The oscillation period is calculated based on a common signal (e.g. inlet pressure, flow rate) recorded simultaneously with the other measurements. Based on the observation at low pressure conditions, the inlet pressure shows one distinguishable valley in every period. The period is thus calculated as the averaged time difference between neighboring valleys. Figure 3(a) shows an example of the valley picking result for a signal measured in one measurement step. Figure 3(b) exhibits the distribution of the time difference between neighboring valleys. In this example condition at 190 kPa, the standard deviation of the distribution in Fig.3(b) is around 0.2 second as marked by the black dashed lines, which is satisfactorily smaller than the magnitude of the oscillation period (17.5 s) marked by the red solid line.

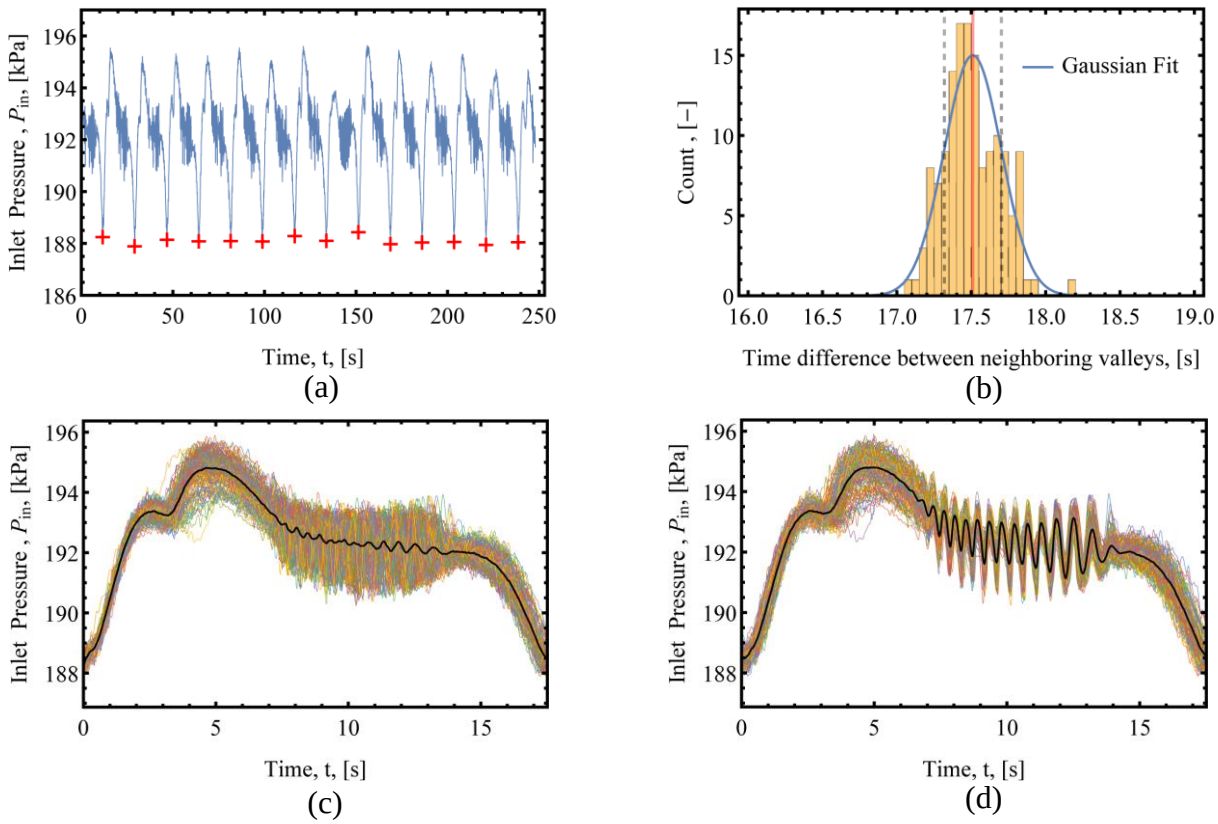

Figure 3: Aligning the oscillation cycles in the inlet pressure signals (190 kPa case). (a) Picking the valleys in the P_{in} signals. (b) The distribution of the time difference between neighboring valleys. (c) Rough alignment of oscillation cycles. (d) Finer alignment of oscillation cycles.

The inlet pressure signals are then partitioned into one-period-long segments each starting at one valley, roughly aligning the cycles by their valleys. Averaging operation is then performed among these segments to obtain the averaged inlet pressure behavior. The colored lines in Fig. 3(c) are 146 roughly aligned segments, while the black line represents the averaged inlet pressure behavior in one period.

Finer alignment is carried out using a cross-correlation based iteration method. The inlet pressure signals are re-partitioned into one-period-long segments such that they begin around the valleys and their cross-correlations with respect to the averaged inlet pressure behavior is locally

maximized. Mathematically, if noting the averaged inlet pressure as $\overline{P_{in}}(\tau)$, the finer alignment of the i-th oscillation cycle is equivalent to finding the proper t_i around the i-th oscillation valley so that the cross-correlation integral below is locally maximized as a function of t_i:

$$\int_0^{t_{period}} \overline{P_{in}}(\tau)\ P_{in}(t_i + \tau)\, d\tau \tag{2.1}$$

where t_{period} is the oscillation period. The new i-th segment is sliced as $P_{in}(t_i + \tau)$ with $\tau \in (0, t_{period})$. The averaged inlet pressure behavior is then re-calculated based on the new segments. This procedure is iterated 4 times to ensure that the different oscillation cycles are well aligned. Figure 3(d) exhibits the finer alignment result after the final iteration.

As the inlet pressure is always measured simultaneously with other parameters, directly applying its partitioning operation to other signals will align the oscillation cycles in all the signals. Figure 4 shows the performance of this method for typical measured parameters. Over 140 periods of inlet velocity signals and over 12 periods of local temperature, differential pressure and void fraction signals are aligned in Fig. 4. To show the oscillation behavior clearly, the results are plotted for two periods. After the alignment, the mean behaviors of all parameters are exported as the post-processing result.

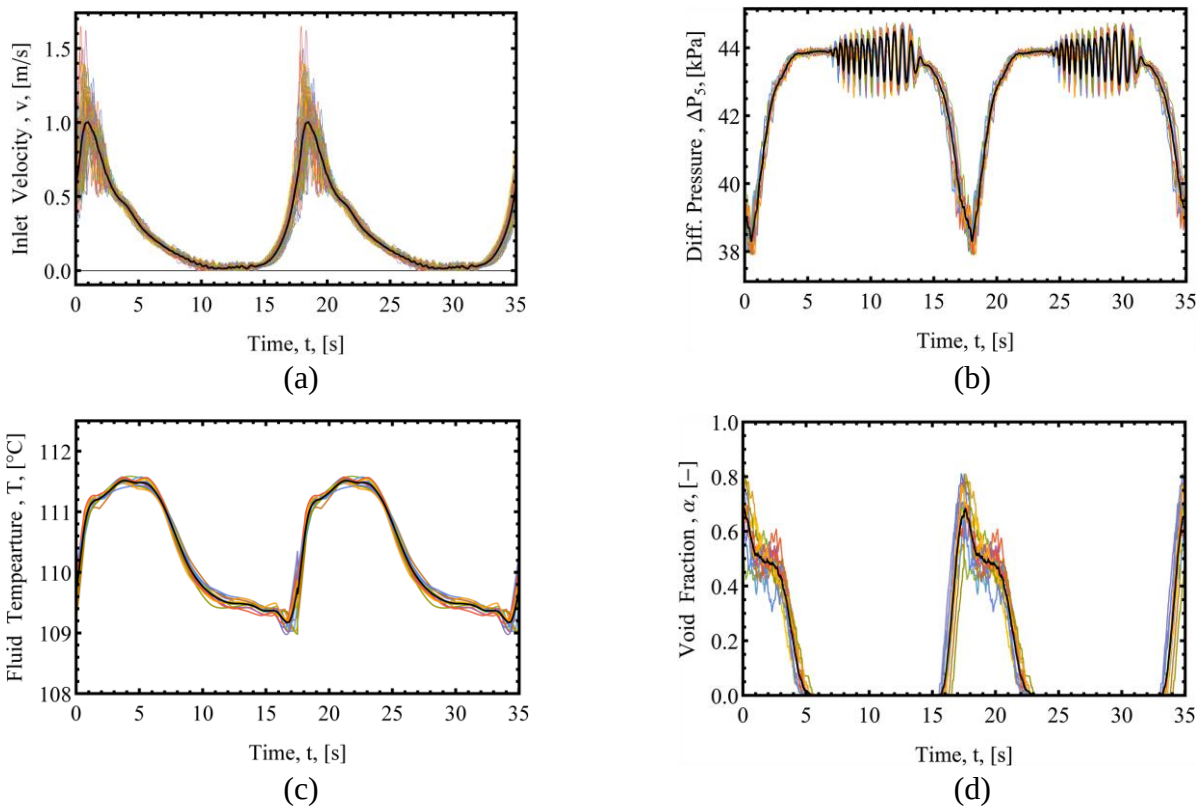

Figure 4: The alignment performance of other parameters. (a) Inlet volumetric velocity. (b) Differential pressure between the inlet and Port 5. (c) Local fluid temperature at Port 5 and $R^* = 0.5$. (d) Local void fraction at Port 5 $R^* = 0.5$.

The local void fraction mentioned above is calculated by applying a moving time-averaging window on the phase indication function measured by the conductivity probes. In order to satisfy the fundamental hypothesis on smoothness of mean values in two-phase modeling [35], the output void fraction is required to be free of small-scale discontinuity and no loss of large-scale transient behavior. The sensitivity study is performed, and one example is shown in Fig. 5. When the window width changes from 0.2 s to 2 s, while the smoothness of the void fraction gets affected significantly when the window width is too small, the overall trend of the void fraction is not very sensitive to the window width. The window width is chosen as 1.4 second because it provides smooth void fraction and keeps the large-scale transient behavior for both the void fraction

measured in one single period and the mean void fraction averaged over multiple periods. The area-averaged void fraction is calculated from the local void fraction assuming angular symmetry over the flow area.

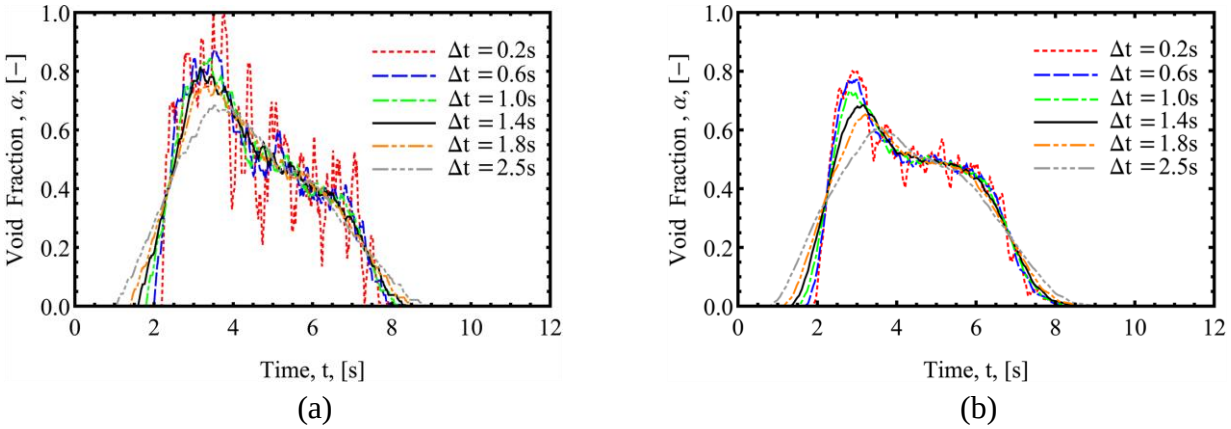

Figure 5: Sensitivity of local void fraction with different time-averaging windows. (a) One-time measured transient signal with different time-averaging window widths. (b) Local void fraction behavior averaged over multiple oscillation cycles with different time-averaging window widths.

The procedure mentioned extracts and aligns the oscillation cycles based on the inlet pressure signals, and this is reliable when the waveform of inlet pressure is simple and clean. For low-pressure conditions (190kPa), distinguishable valleys appear in the inlet pressure signals with the same period of the system oscillation, so the inlet pressure is chosen to indicate the system's oscillation phase. These valleys originate from steep void fraction jumps in the adiabatic riser. However, under higher pressure (500kPa), due to smoother void fraction change and reduced oscillation magnitude, random noises and small fluctuations blur inlet pressure signals, Fig. 6(a). Therefore, for cases recorded at 500kPa, post-processing is performed using the inlet flow rate signals due to the clarity of valley identification, Fig. 6(b). Figure 7 compares the distributions of time difference obtained after valley identification and finer alignment using the inlet pressure

(Fig. 7(a)(b)) and the inlet velocity (Fig. 7(c)(d)) at 500 kPa. The valley identification result of inlet pressure signals shows larger deviation in the time difference between valleys than that of inlet velocity. While the performance of finer alignment based on the inlet pressure is unsatisfactory because of the blurred waveform with high frequency noises and fluctuations, the finer alignment using the inlet velocity shows less than 0.3 s of the standard deviation in the time difference between neighboring cycles' beginnings. Generally, parameters recorded in all measurement steps and exhibit clear oscillation patterns should be used for extracting the oscillation cycles.

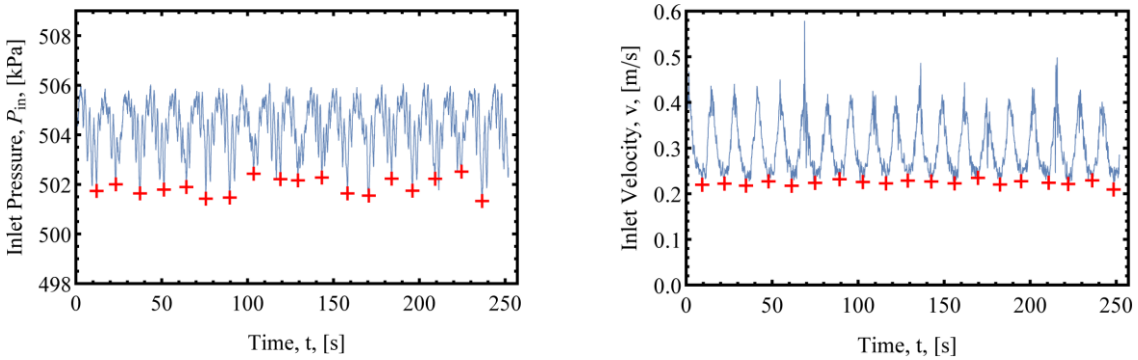

Figure 6: Typical raw signals of the inlet pressure and inlet velocity at 500kPa. (a) Inlet pressure signal. (b) Inlet velocity signal. The red markers are the result of valley identification. In (a), valley identification can be ambiguous because of the local minima introduced by fluctuations with relative higher frequency than the oscillation of the system.

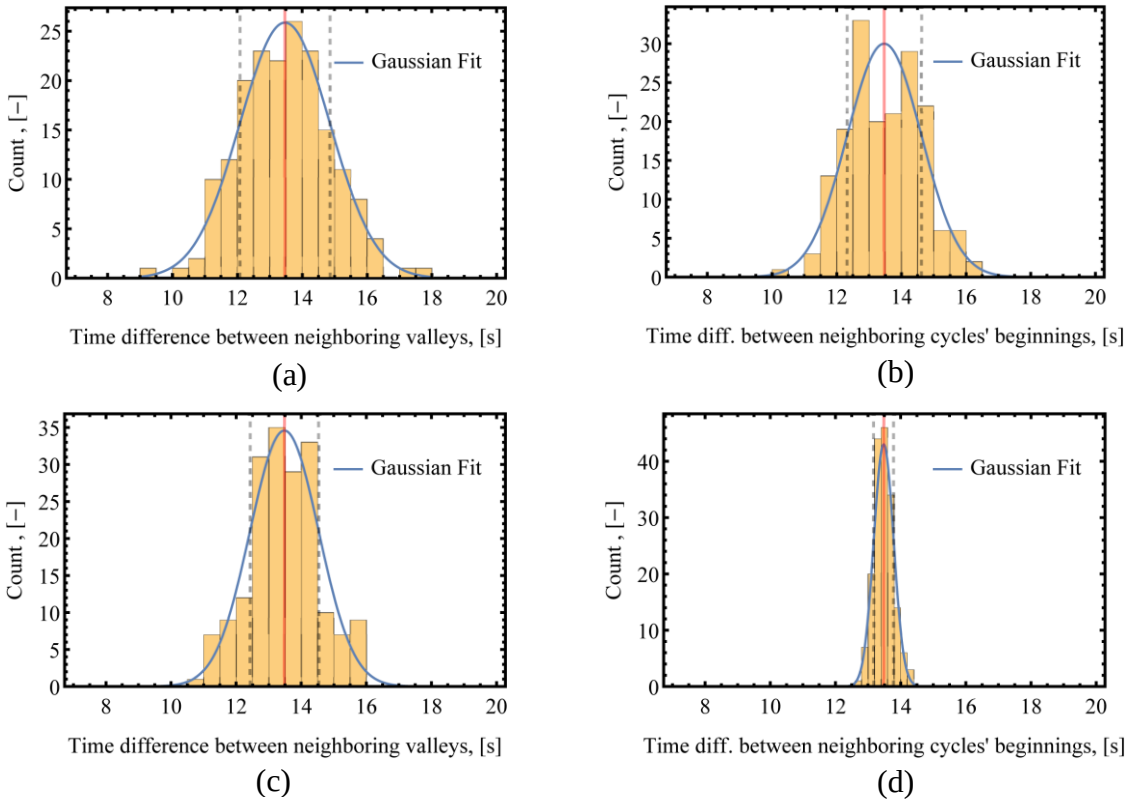

Figure 7: The processing performance using inlet pressure and inlet velocity at 500kPa. (a) Distribution of time difference between neighboring inlet pressure valleys. (b) Distribution of time difference between neighboring cycle's beginnings obtained from the finer alignment based on the inlet pressure. (c) Distribution of time difference between neighboring inlet velocity valleys. (d) Distribution of time difference between neighboring cycle's beginnings obtained from the finer alignment based on the inlet velocity.

CHAPTER 3: RESULT AND DISCUSSION

3.1 Stability Maps

On the same facility, tests covering a large operation range have been performed by Ooi et al. [33] in a previous project aiming at a comprehensive steady-state two-phase natural circulation dataset. During the tests, several conditions exhibiting instability were encountered especially under low system pressure. These unstable conditions, together with the steady-state natural circulation dataset, provide valuable stability data for the current research. Based on these tests' result, stability maps are drawn on non-dimensional Zuber-subcooling planes (Fig. 8(a)) and also dimensional planes (Fig. 8(b)) to exhibit general stability characteristics of the experimental loop. Some maps in Fig. 8(a) do not have unstable cases, the purpose of showing them is to exhibit the parametric effects of K_{loss} on the stability of the system and on the operational conditions' locations in the dimensionless stability map.

In Fig. 8(a), the subcooling number N_{sub} and the phase change number (the Zuber number) N_{pch} are defined with time-averaged parameters at the test section inlet as:

$$N_{sub} = \Delta i_{sub,in} \left(\frac{\Delta \rho_{fg}}{\rho_g \Delta i_{fg}} \right)_{sat,in} \tag{3.1}$$

$$N_{pch} = \frac{Q}{W} \left(\frac{\Delta \rho_{fg}}{\rho_g \Delta i_{fg}} \right)_{sat,in} \tag{3.2}$$

Conditions with zero vapor quality at the exit of the adiabatic chimney $x_{ch,exit} = 0$ are given by the orange lines in Fig. 8(a):

$$N_{pch} - N_{sub} = -\left(i_{sat,f,in} - i_{sat,f,ch,exit} \right) \left(\frac{\Delta \rho_{fg}}{\rho_g \Delta i_{fg}} \right)_{sat,in} \tag{3.3}$$

where the pressure at the exit of the adiabatic chimney is obtained from linear extrapolation.

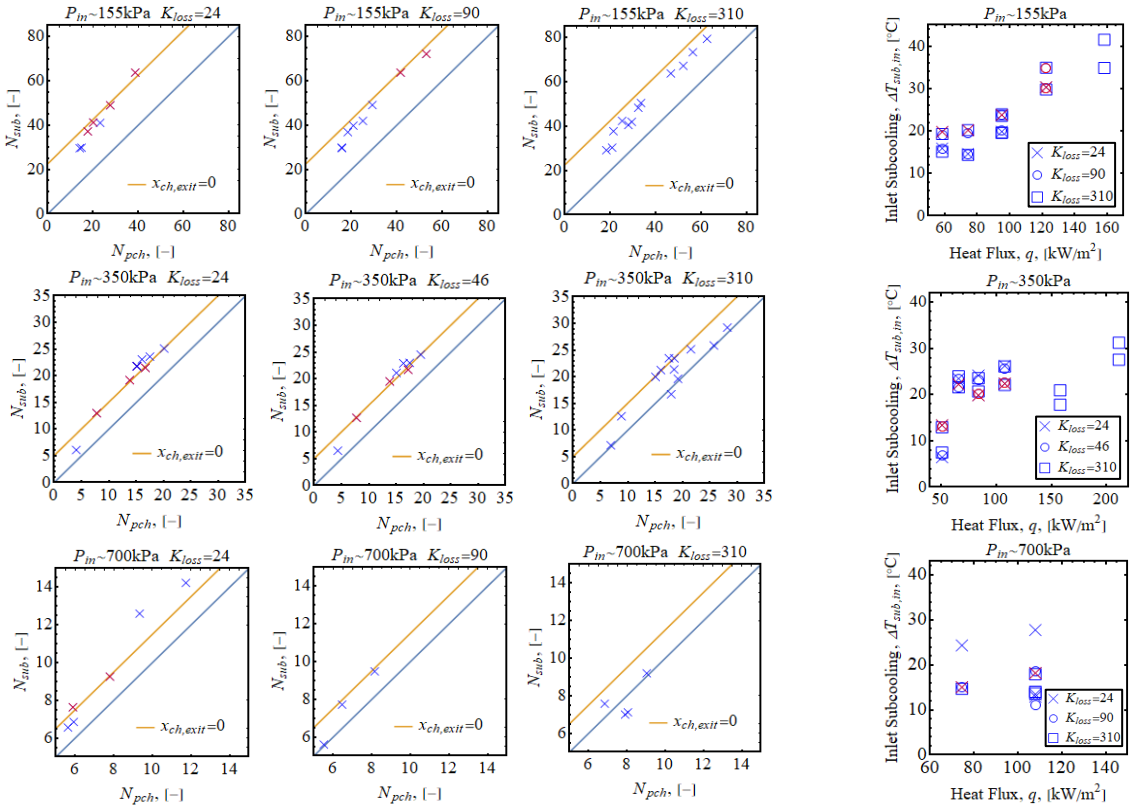

Figure 8: Stability maps based on the steady-state tests [33]. Unstable cases are marked by red and stable cases are marked by blue. (a) On non-dimensional planes. (b) On dimensional planes.

Instability is found to occur when the vapor quality at the exit of the adiabatic chimney is close to zero as shown in Fig. 8(a). This is consistent with the characteristics of the Type-I density wave oscillation as classified by Fukuda et al. [13]. It also indicates that the phase change in the adiabatic chimney plays an important role in inducing the instability. For these conditions, even though the fluid at the exit of the heated section is subcooled, the dropping of hydrostatic pressure along the vertical adiabatic chimney can cause the saturation temperature to drop below the temperature of the fluid travelling upward, which introduces rapid vapor generation known as the flashing. The resultant steep change in void fraction perturbates the driving force of natural circulation significantly and introduces strong feedback effects, which is found by many researchers [15, 21, 23] to be a dominant driving mechanism for the instability under low pressure.

The stability maps also show parametric effects on the system's stability. Generally, the instability happens when the exit of the chimney has nearly zero vapor quality, and therefore either increasing or reducing the vapor quality is possible to result in a stable operation condition. The inlet flow restriction has a stabilizing effect, i.e. increasing K_{loss} is effective in stabilizing the flow conditions. It is also found that the decreased flow rate resulted from the increased K_{loss} can move operation conditions on the non-dimensional stability Zuber-subcooling plane to higher N_{pch}.

Based on the stability maps, the current experiment is then performed under the procedure described in Chapter 2 aiming at capturing detailed instability phenomena. Periodic oscillations are captured for conditions with nearly zero vapor quality at the exit of the test section. The results after post-processing are discussed in the following sections.

3.2 Example Data and Cyclic Phenomena

Examples for the reconstructed oscillation are shown in Figs. 9, 11, 12. Waveforms over two periods are plotted for clarity in exhibiting the system's behavior. Saturation temperatures at five measurement ports are calculated from the absolute pressure and are plotted as long-dash lines. The radial location of the measurement points is marked by the non-dimensional radial location $R^* = (r - R_i)/(R_o - R_i)$, where R_i and R_o are the inner and outter radii of the test section. Cyclic phenomena in one example oscillation are shown and described in detail. Comparison between two distinct patterns for flow oscillation at lower pressure (190kPa) are performed. An example condition at 500kPa is analyzed to cover conditions at higher system pressure. These example conditions show the ability of the proposed method in capturing oscillating phenomena and are representative of the conditions covered by the dataset.

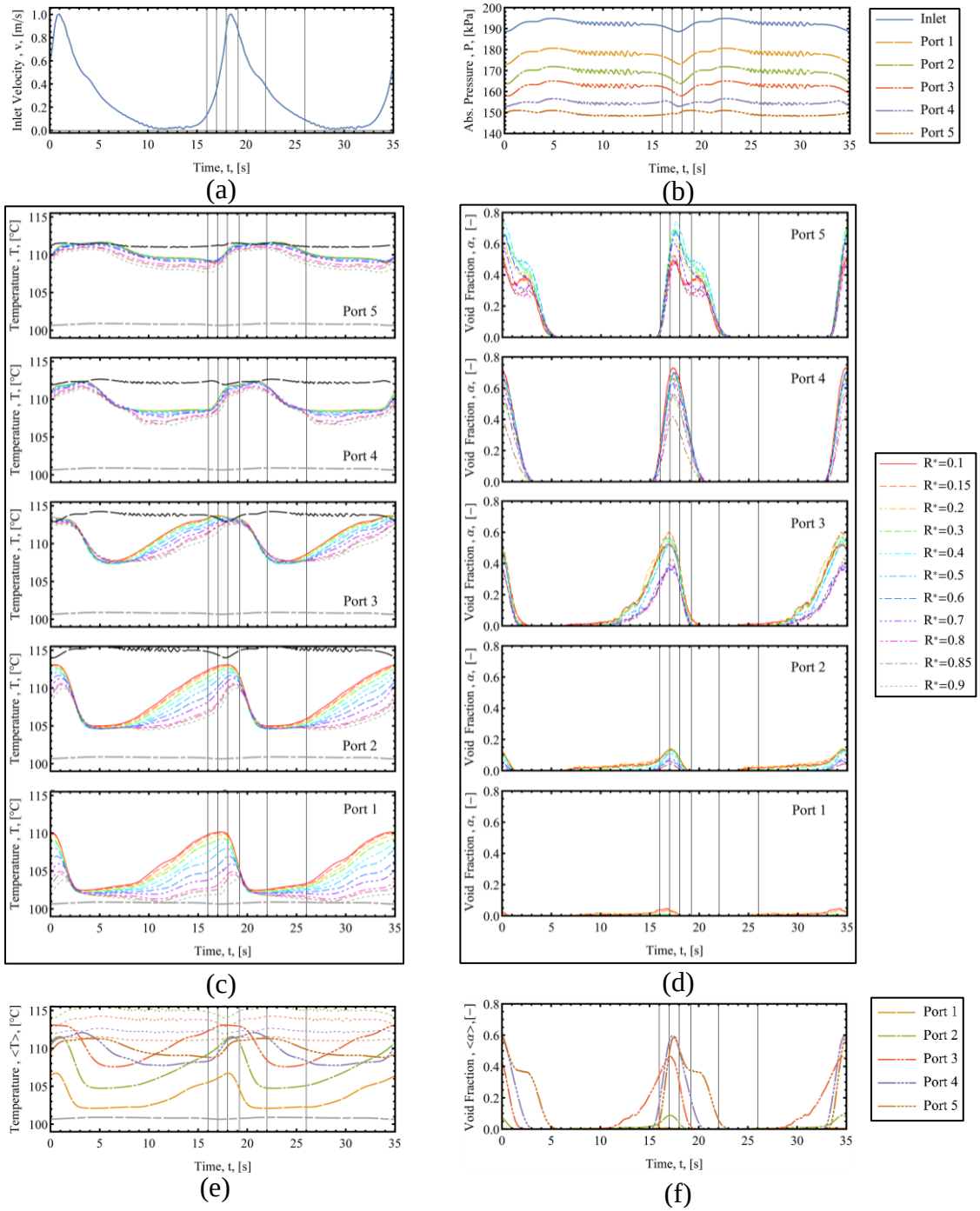

Figure 9: An example of the reconstructed oscillating condition (P_{in} = 192kPa, $\Delta T_{sub,in}$ = 18.4°C, q = 45.4kW/m^2, K_{loss} = 22). (a) Inlet volumetric velocity. (b) Absolute pressure. (c) Local fluid temperature. (d) Local void fraction. (e) Area-averaged fluid temperature. (f) Area-averaged void fraction. Black long-dash lines in (c) and short-dot lines in (e) are the saturation temperature. Gray long-dash-short-dash lines in (c) and (e) are the inlet temperature. Legends for different locations are shared by (c) and (d), (e) and (f).

Cyclic phenomena induced by instability are revealed by the post-processed data, Fig. 9. At a given time, near the heating wall at the end of heated section, the fluid gets close to saturation and vapor generation increases, Fig. 10(a). As the flow rate increases, the fluid with relatively high enthalpy moves downstream and becomes saturated due to the decrease of hydrostatic pressure, which induces the rapid vapor generation, or flashing, close to the inlet of the chimney, Fig. 10(b). The void generated propagates downstream, causing the sudden rising of void fraction at Port 4 and 5, Fig. 9(f). The resultant loss of hydrostatic pressure drop in the chimney causes a large jump in the driving force, leading to further acceleration of flow rate, Fig. 9(a). The higher flow rate pushes more high-enthalpy fluid into the chimney, which leads to the propagation of flashing from Port 3 to the whole chimney, Fig. 10(c). However, high flow rate in turn reduces the resident time of fluid in the heating section, which reduces the enthalpy of the fluid entering the chimney, Fig. 10(d). After some delay, vapor generation is subsequently suppressed from Port 3 to Port 5, Fig. 10(d-e), and the flow rate decreases to a relatively low value gradually. The system thus returns to a low flow rate state allowing the fluid in the heating section to build up high enthalpy, Fig. 10(f). The phenomena observed in the experiment is consistent with the general mechanism of flashing-induced instability proposed in literature [21].

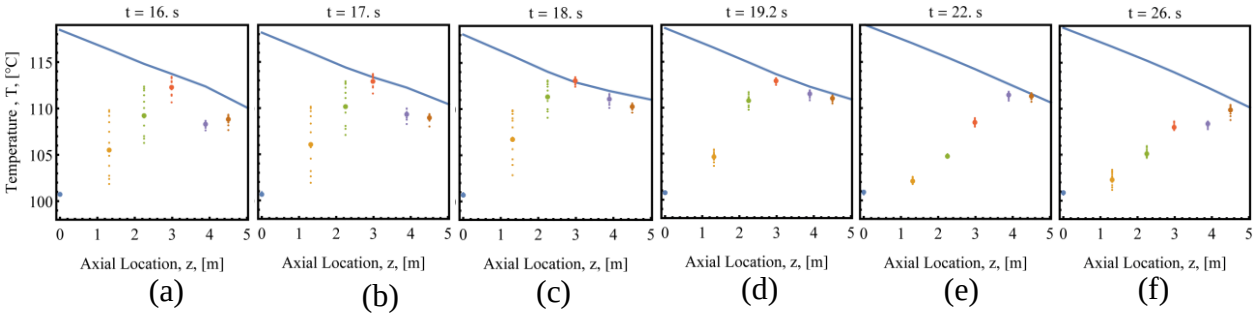

Figure 10: Snapshots showing the temperature evolution. The condition is the same as in Figure 9. The solid lines are the saturation temperature interpolated from the measured pressure. Small points are the local fluid temperature while large points markers the area-averaged temperature. The instants are also marked by the vertical lines in Figure 9.

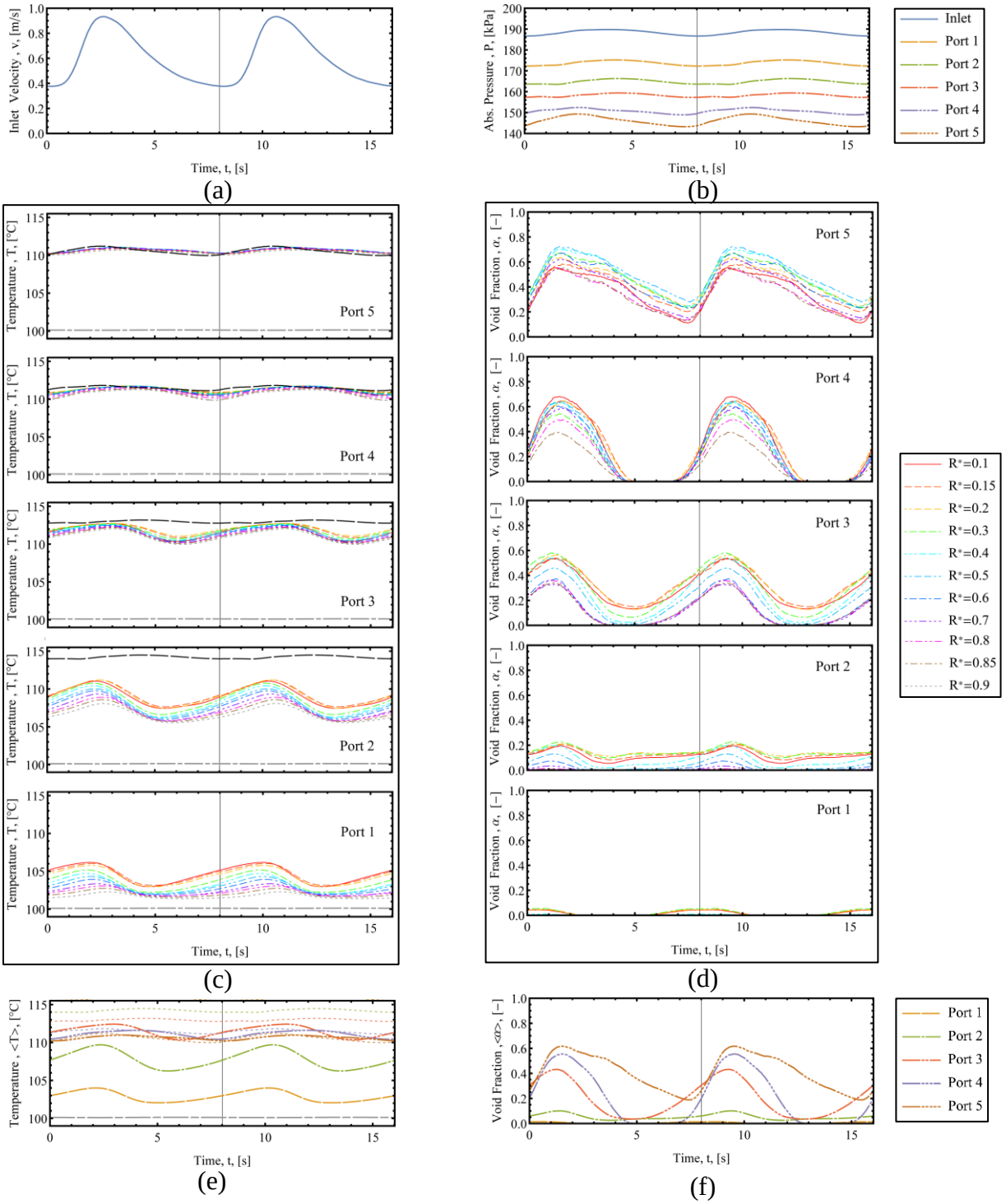

Figure 11: An example condition where the top of the test section is always in two-phase. (P_{in} = 188kPa, $\Delta T_{sub,in}$ = 18.2°C, q = 134.8kW/m^2, K_{loss} = 22). (a) Inlet volumetric velocity. (b) Absolute pressure. (c) Local fluid temperature. (d) Local void fraction. (e) Area-averaged fluid temperature. (f) Area-averaged void fraction. The definition of lines is same as in Figure 9.

The example condition in Fig. 9 shows intermittent flow rate oscillation also reported in other experiments [14-15, 21, 23]. The evolution of temperature and void fraction indicates that flashing happens intermittently and the flow in the adiabatic chimney alternates between single-phase and two-phase. The flow rate peaks recur periodically at the same time when flashing happens and induces large change in the gravitational pressure drop. Low-flow-rate time intervals without significant flow rate change are clearly observed between the neighboring flow rate peaks when the top of the adiabatic section is in liquid-phase and the heated section is building up high enthalpy. Another commonly reported oscillation pattern, which is characterized by continuous two-phase flow at the top of the chimney, is also observed in conditions with relatively lower inlet subcooling or higher heat flux, Fig. 11. Temperature and void fraction measurement directly show that the flow above port 5 is always saturated and contains two phases. The void fraction at port 5 is always higher than at port 4, showing that the flashing induced void generation inside the adiabatic chimney contributes significantly to the driving force of the flow oscillation. The existence of an oscillating boundary in the adiabatic chimney between the two-phase and signal-phase regions is indicated by the fact that non-zero void fraction is intermittently detected at port 4 but continuously appears at port 5. The axial void distribution at t = 5.5s shows the flow alternates in space between single-phase and two-phase three times, indicating that subcooled single-phase flow, subcooled boiling, condensation and flashing can happen in the test section simultaneously dominating at different regions. The radial distributions of void fraction indicate that the flow pattern changes from port 1 to port 5, adding more challenges to the modeling and the simulation of this oscillation. The flow rate, compared with the intermittent oscillation pattern, fluctuates continuously with relatively shorter period, and its waveform has higher minima and resembles a sine function.

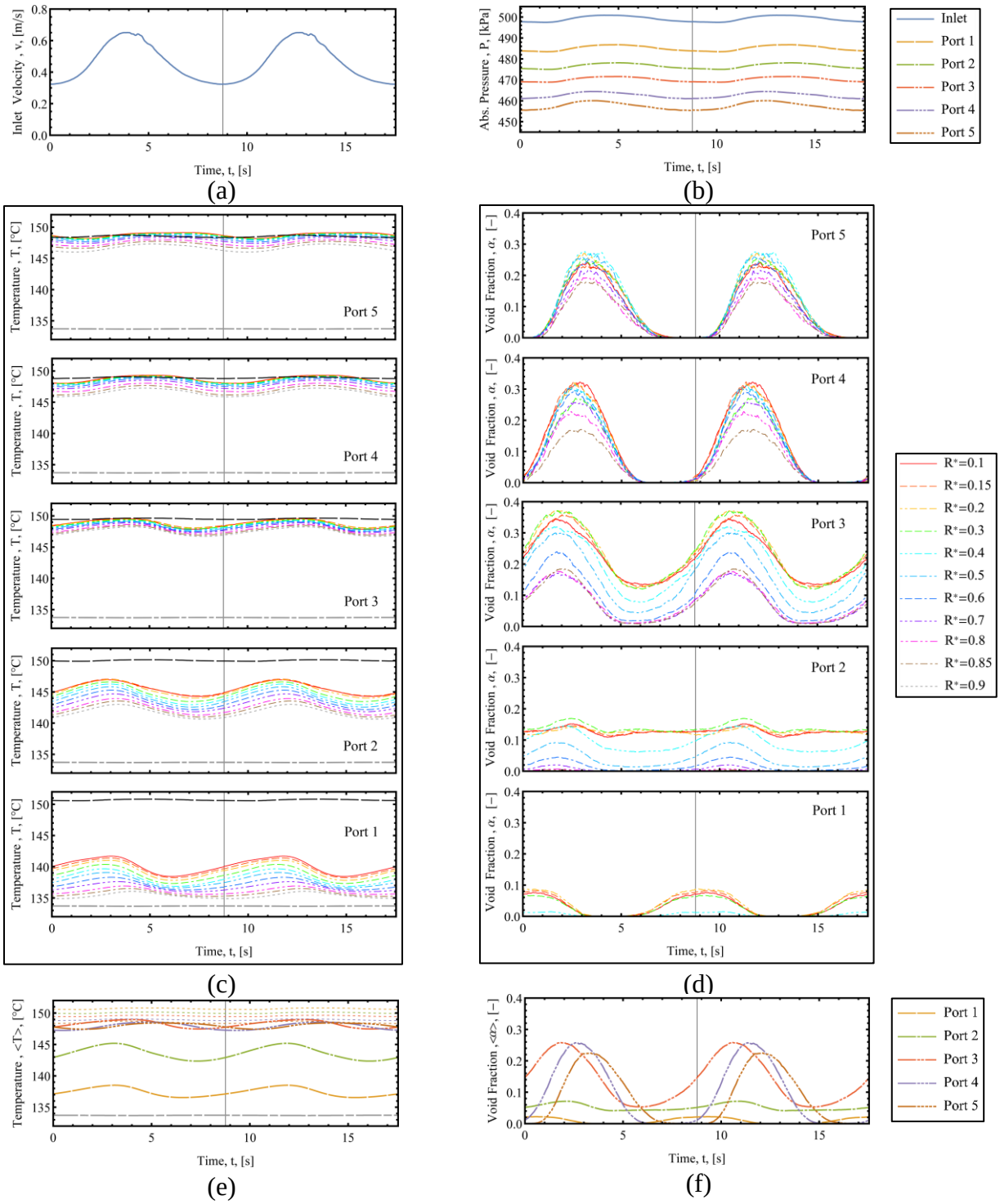

Figure 12: An example condition at 500kPa. (P_{in}=499kPa, $\Delta T_{sub,in}$=18.1°C, q=134.8kW/m^2, K_{loss}=22). (a) Inlet volumetric velocity. (b) Absolute pressure. (c) Local fluid temperature. (d) Local void fraction. (e) Area-averaged fluid temperature. (f) Area-averaged void fraction. The definition of lines is same as in Figure 9.

An example oscillation at higher pressure (500kPa) is shown in Fig. 12. The cyclic phenomena are similar to those at lower pressure. Vapor generation increases when the fluid at the heated section outlet gets close to saturation, leading to the flow rate increase which in turn reduces the enthalpy and dampens the vapor generation as a delayed feedback. Compared with the 190kPa cases, the void fraction, which can strongly influence the driving force of two-phase natural circulation, shows lower magnitude. The saturation temperature drops much slower with the decreasing hydrostatic pressure, and the flashing becomes less significant in generating vapor. In the example condition, the void fraction peak shows no obvious increasing trend from port 4 to port 5 even though the local temperature close to the inner wall can reach the saturation temperature. The effect of condensation is observed near the outlet of the heated section where the void fraction exhibits clear reducing trend from port 3 to port 4, which is not obvious from port 4 to port 5. The decreasing hydrostatic pressure in the adiabatic chimney does not induce significant void generation as at low pressure, but still contributes to compensate the effect of condensation. Due to less phase change, the travelling void fraction wave is more clearly observed from port 3 to port 5, highlighting the time delay effect introduced by the adiabatic chimney, The high enthalpy fluid carrying void needs to travel through adiabatic chimney before its contribution to the driving force of natural circulation can be lost, which contributes to the out-of-phase feedback between the enthalpy and the flow rate. Generally, at higher pressure (500kPa), the vapor generation from flashing is less significant compared to lower pressure, and the waveforms exhibit lower fluctuation amplitude and smoother shapes.

3.3 Parametric Effects

Parametric effects within the experiment range are summarized in this section. The analysis is based on both the reconstructed periodic oscillations and other conditions encountered during the operation of the facility. Inlet flow rate behaviors are plotted to exhibit the general trend in the stability and the characteristics of the oscillations. In these figures, raw signals are drawn for non-periodic cases, and post-processed data are used for periodic conditions.

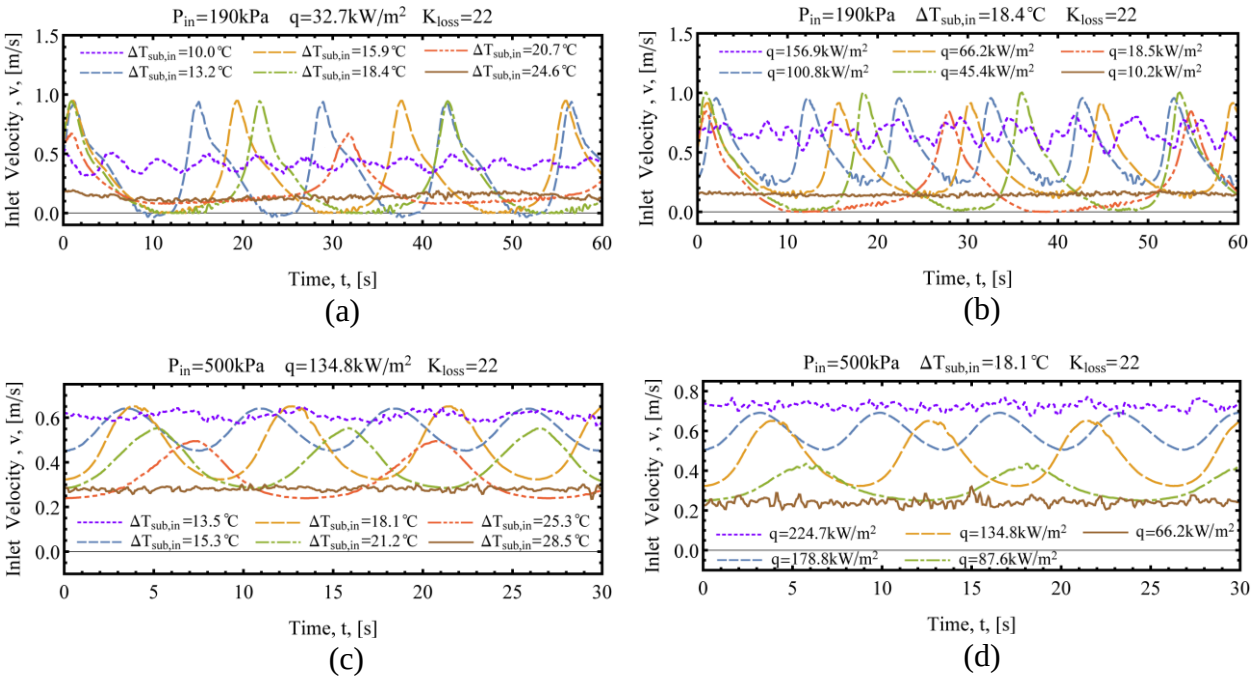

Figure 13: Parametric effects of the inlet subcooling and the heat flux. (a) Parametric effects of the inlet subcooling (190kPa). (b) Parametric effects of the heat flux (190kPa). (c) Parametric effects of the inlet subcooling (500kPa). (d) Parametric effects of the heat flux (500kPa).

Reducing the inlet subcooling and increasing the heat flux have similar effects on the stability behavior of the system. From a stable single-phase natural circulation condition, the system can cross an unstable condition-range by either reducing the inlet subcooling or increasing the heat flux. As shown in Fig. 13, during this process, the system first experiences oscillations

induced by the intermittent flashing in the adiabatic chimney, and the oscillation magnitude increases because of enhanced flashing. The oscillation period then decreases, and the flashing happens more frequently. The intermittent void fraction peaks in the adiabatic chimney become closer and finally merge with each other, and another oscillation pattern then happens with continuous two-phase flow as mentioned in Section 3.2. In the flow rate waveform, the peaks also merge, which increases the minimum flow rate and reduces the oscillation magnitude. Further reducing the inlet subcooling or increasing the heat flux will result in stable conditions with stable two-phase flow in the chimney. Generally, the oscillation period decreases monotonically with reducing inlet subcooling or increasing heat flux, while the oscillation magnitude first increases and then decrease.

There is also difference in the parametric effects of the inlet subcooling and the heat flux. As shown in Fig. 13(a), with fixed heat flux, there is a range of inlet subcooling leading to intermittent oscillations with a common shape for their flow rate peaks. For these cases, reducing the inlet subcooling influences the oscillation waveform mainly by shrinking the time interval with low flow rate, or the "incubation period" [15, 20] for the heated section to restore high enthalpy fluid. While the incubation period changes considerably, the shape of the flow rate peak is not obviously influenced by the inlet subcooling within this range. However, for the intermittent oscillations with fixed inlet subcooling, the magnitude and the shape of the oscillation tend to be influenced by the heat flux, Fig. 13(b). A possible explanation is that the incubation period is dominated by the single-phase natural circulation where the heat flux has more direct effect than the inlet subcooling on the enthalpy distribution and the flow rate.

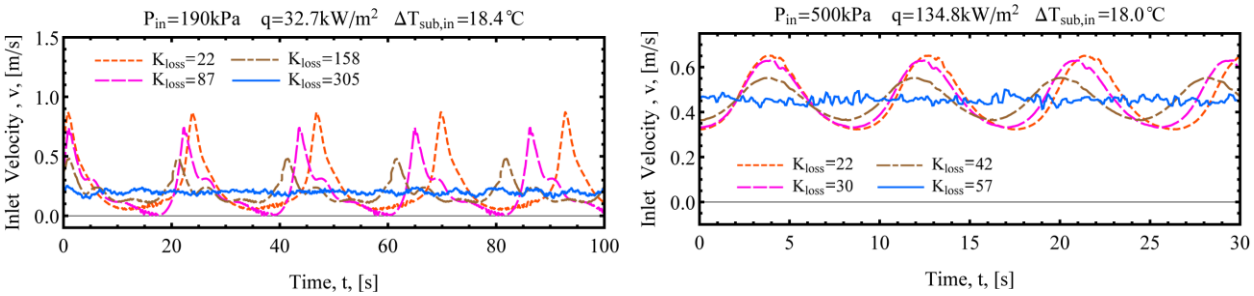

Figure 14: Parametric effects of the inlet pressure loss coefficient K_{loss}. (a) Parametric effects of the inlet flow restriction (190kPa). (b) Parametric effects of inlet flow restriction (500kPa).

The inlet flow restriction shows stabilizing effect in the current experiment range. From an unstable condition, increasing the inlet pressure loss coefficient K_{loss} dampens the oscillation magnitude and finally results in a stable condition, Fig. 14. The oscillation period is not influenced significantly compared with the large relative change in the oscillation magnitude. The shape of the oscillation is also impacted, which is more obvious at lower pressure. This stabilizing effect is similar to the situation in the density wave oscillation [1, 9], and it can be explained by the increasing of the single-phase friction drop which is in-phase with the inlet flow rate and dampens the oscillation. Marcel et al. [16] report the inlet restriction to be destabilizing based on systematic tests covering large operation ranges. It should be noted that their conclusion focuses on the behavior of the stability boundary on the subcooling-power plane. Higher flow restriction is found to result in lower flow rate and thus higher inlet subcooling for the onset of the flashing and the flashing-induced instability. The inlet flow restriction is concluded to be stabilizing because of its damping effect on the oscillation.

The phenomena cycles and the parametric effects mentioned are consistent at 190kPa and 500kPa. At high pressure, the instability occurs within a narrower range of conditions, and the oscillations are smoother and with lower amplitude. At 500kPa, the instability only occurs above a minimum inlet subcooling and a minimum heat flux for the conditions tested. If the inlet subcooling or the heat flux is too low, no self-sustainable oscillation happens even when the flow in the adiabatic chimney changes from single-phase to two-phase flow with saturated mixture occupying the end of the test section. This is consistent with the stability maps reported by Furuya et al. [11]. Compared with low pressure conditions, the oscillation waveforms at high pressure have smaller amplitudes and more regular shapes. Intermittent flashing can still be observed in periodic oscillations, but the void-fraction does not increase as significantly as at low pressure, and the flow rate waveform is close to the sine function. Consistent with the accepted understanding in literature [11, 15-16, 19], increasing the system pressure is stabilizing.

3.4 Oscillation Period and Fluid Particles' Residence Time

Research on flashing-induced instability reports close relationships between the oscillation period and the time for a fluid particle to travel through the channel. Furuya et al. [21] claim that the oscillation period is about 1.5 to 2 times of the passing time of liquid in the adiabatic chimney, which is calculated as the chimney's volume divided by the averaged inlet volumetric flow rate. Manera et al. [15] report that the period is around twice the time for a particle with averaged inlet flow rate to pass half of the heated section and a whole adiabatic riser. Marcel et al. [16] report the similar finding for both experiments and numerical results. The travelling times are viewed as the characteristic transit time for perturbations to propagate in the loops, and their relationships with the oscillation period are thus reported to be similar to those in the density wave oscillation.

In the current study, the time for the two-phase mixture to travel through the test section is calculated based on the velocity given by the one-dimensional mixture continuity equation:

$$\frac{\partial \rho_m}{\partial t} + \frac{\partial}{\partial z}\left(\rho_m v_m\right) = 0 \tag{3.4}$$

where the density of two-phase mixture is $\rho_m(z,t) = \langle\alpha\rangle \rho_g(P,T) + (1-\langle\alpha\rangle)\rho_f(P,T)$. Experimentally measured inlet velocity $v(t) = v_m(z=0,t)$, void fraction $\langle\alpha\rangle$, fluid temperature T and pressure P are input to calculate ρ_m and $\frac{\partial \rho_m}{\partial t}$ at the inlet and five ports. The values of $\frac{\partial \rho_m}{\partial t}$ between neighboring measurement locations is approximated by linear interpolation, and the value of $\frac{\partial \rho_m}{\partial t}$ between the last measurement port and the outlet of the test section is approximated by the value at the last measurement port. The mass flux $\rho_m v_m$ is then solved by direct integration. The mixture velocity v_m is calculated at five ports. Interpolation and extrapolation operations similar to those for $\frac{\partial \rho_m}{\partial t}$ are performed for v_m. The motion of fluid particles entering the heated section at different instants t_0 is then traced as $z(t,t_0) = \int_{t_0}^{t} v_m(z(t',t_0),t') \cdot dt'$. Averaged residence time in the test section is finally calculated for all fluid particles weighted by their mass or $v(t_0)dt_0$ equivalently.

The lines in Fig. 15(a) represent the traced motions of particles with a same mass for the same example condition in Fig. 9. The comparison between the oscillation period and the averaged residence time in the test section is plotted in Fig. 15(b).

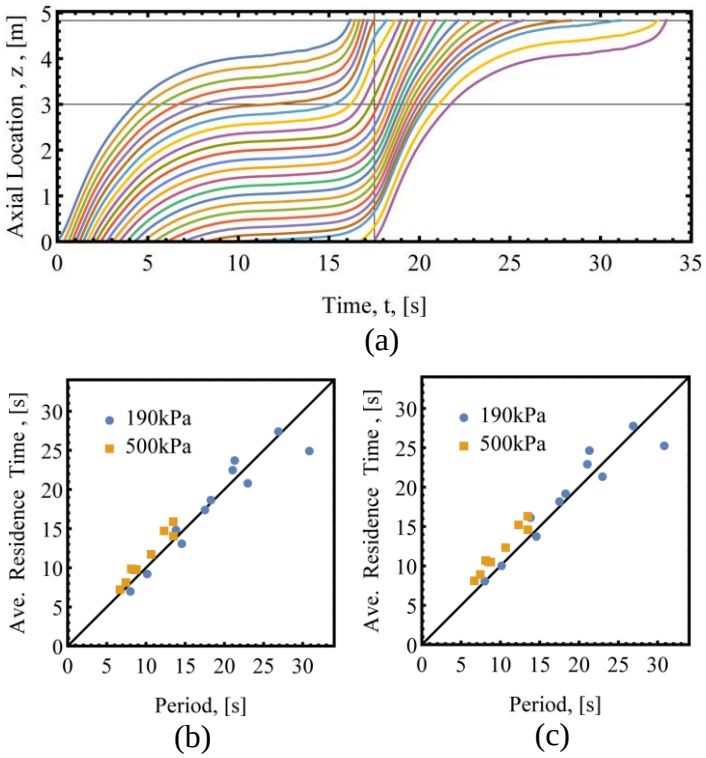

Figure 15: Comparison between the oscillation period and the averaged residence time. (a) The motion of particles entering the test section in one period. (b) The oscillation period and the averaged residence time in the test section calculated based on two-phase mixture's motion. (c) The oscillation period and the estimated averaged residence time in the test section calculated with the mean inlet flow rate.

The traced motion shows that the residence time of an individual particle generally depends on the time when the particle arrives at the inlet. For the example case shown in Fig. 15(a), the longest residence time is around 21s corresponding to the particle entering the test section at t = 10s, while the shortest residence time is about 16s belonging to the particle entering the test section around t = 0s. However, for the major part of the particles, their deviation in the residence time is very small compared with the magnitude of the averaged residence time. These particles enter the test section rapidly when the inlet flow rate experiences its peak, so they take up a large amount of mass and thus a significant weight in the averaging procedure. For those particles arriving at

the test section with a low velocity, they usually also leave the test section slowly, and their residence time can vary a lot compared with other particles. This feature is especially obvious in those low-pressure cases with short periods where the flow peak is strong and incubation time is short.

In the current experiment range, the averaged particle residence time in the test section is approximately equal to the oscillation period. The averaged particle residence time is dominated by the fluid particles entering the test section during the flow rate peak. This insurgence flushes out the high enthalpy fluid in the hot side, resetting the system to a flow with relatively low enthalpy, and then stay in the test section until next flow rate jump. The period is thus qualitatively related to the time for the low enthalpy fluid to refill the hot side and the time for the heated section to restore sufficient enthalpy for triggering flow rate increase and vapor generation.

The residence time can also be estimated as the length of the test section divided by the averaged inlet flow velocity, which gives the values in Fig. 15(c). Comparing Fig. 15(b) and (c), the difference in the averaged residence time given by these two methods are satisfactorily small compared with the magnitude of the oscillation period. The reason is that the two-phase flow only dominates in the chimney and during the relatively short time interval when high enthalpy fluid carries large amount of void. Hence, the difference between the mixture velocity and the inlet velocity is only considerable for the fluid particles near the test section exit and during the flow rate peak. The resultant difference in the residence time is thus limited because it has a small numerator (distance) and a large denominator (velocity). Based on this finding, estimating the travelling time of fluid particles using averaged inlet flow rate is precise enough for comparison with the oscillation period.

The characteristic time scales reported in literature are also verified. The oscillation period is about 2.7 times of the passing time of liquid in the chimney, and this discrepancy with Furuya et al.'s 1.5 to 2 times the chimney residence time [21] may be reasoned by the different facility geometries. Different from the SIRIUS-N facility whose adiabatic chimney takes around 90% of the test section volume, the chimney section of the current facility only takes up about 40% of the total length of the test section. The chimney height is not a proper length scale for estimating the transit time of perturbations in the current loop. Using the calculation method of Manera et al. [15], the oscillation period is about 1.5 times the transit time, which falls within the range of 1.5 to 2. The propagation time of enthalpy perturbation and the oscillation period show similar relationships as in the density wave oscillation.

CHAPTER 4: CONCLUSIONS AND FUTURE WORK

4.1 Conclusions

In this research, periodic oscillations induced by two-phase instability are recorded in a natural circulation loop with an adiabatic chimney above the heated section. Local void fraction and fluid temperature are directly measured by conductivity probes and thermocouples mounted on high-precision traversing mechanisms. The post-processing method reconstructs the periodic system behavior as multi-dimensional time-dependent data, which performs averaging over multiple periods and allows the estimation and reduction of the random error.

The stability maps are drawn with a separate dataset from previous tests on the same facility, which indicates that the instability is encountered when the vapor quality at the test section outlet is close to zero. Detailed phenomena are then revealed by post-processed data from the current experiment. Under low pressure, flashing in the adiabatic chimney induces rapid void fraction change, which is identified phenomenologically to be a dominant contribution to the oscillation.

Heat flux and inlet subcooling show similar parametric effects on the system's stability and the oscillation's waveform. Within the experiment range, inlet flow restriction is found to be stabilizing by dampening the oscillations. Increasing the system pressure can generally stabilize the system by narrowing the unstable operation region and smoothing the oscillation's waveform.

In the current experimental setup, tracing the two-phase mixture's motion based on the continuity equation shows that the oscillation period is close to the average time for the fluid particles to travel through the test section. Comparison shows that the residence time of fluid particles simply estimated with the averaged inlet flow rate is precise enough for comparing with the oscillation period. Other proportional relationships between the period and fluid's residence times are reported in literature and confirmed in this study.

4.2 Future Work

The dataset collected in this research is valuable for the validation of analytical models and computational codes. Researchers have made attempts in predicting the stability boundary of two-phase natural circulation by linear perturbation methods[36-38] and lumped models [16, 39], and experimental stability maps are usually required for the validation of these analytical stability boundaries. Detailed system behavior under instability, such as the self-sustainable limit cycle oscillations reconstructed in the current experiment, is valuable for the validation of the 1-D simulation codes in predicting the transient conditions after the occurrence of instability. Moreover, provided the multidimensional data, the validation of CFD codes in simulating transient two-phase flow with prescribed realistic periodic boundary conditions is also a challenging and interesting topic. The results of these possible validation studies may introduce more fundamental questions on the adaptability of current correlations and models under transient two-phase conditions.

Measurement of two-phase parameters under transient conditions is also a promising future topic which can be performed with the raw data from the current experiment. The four-sensor-conductivity probe have been designed and validated for the steady-state measurement of important two-phase parameters such as void fraction, gas velocity and interfacial area concentration [40-42]. Under transient conditions, while the void fraction is obtained through a simple running average operation from the directly measured phase indication function, other parameters can involve more complicated bubble identification in signal processing and more restrictive statistical requirement. The counting rate of bubbles and interfaces can be time-dependent in transient conditions. There is no prior guarantee for the existence of a suitable time-window which can capture sufficient bubbles by one-time measurement for the measured values to be statistically representative without smoothing out the large-scale transient behavior.

Sensitivity study as performed in Section 2.3 for the void fraction may be required to check the existence of and determine a proper window width, where the ensemble average operation enlarges the sampling size significantly and provides the reliable estimation for the required statistically representative values. Also, there is no guarantee that the window-width is a constant for all time instants, which may further lead to the development of an adaptive method in choosing window-width which changes with time. These possible future works are critical for expanding the measurement ability of four-sensor conductivity probes from steady-state to periodic or even more general transient conditions.

The current experiment method is potentially applicable to capture more periodic two-phase conditions. As shown in Section 3.3 Fig. 14(a), at relatively low pressure (190kPa), the oscillation of flow rate exhibits more complex waveforms with higher inlet pressure loss coefficient K_{loss}. More experiments capturing this type of waveform can be helpful in explaining the distorted oscillation shape and in discovering additional dominating phenomena in two-phase natural circulation. Periodic oscillations under other conditions, such as the Type-II density wave oscillation which typically happens in two-phase forced convection with higher vapor quality [13], can also be recorded as a valuable dataset for transient two-phase flow. Generally, the proposed measurement strategy and post-processing method can be used in capturing more periodic conditions which can enrich the knowledge base of two-phase thermohydraulic study.

REFERENCES

[1] Boure, J., Bergles, A., & Tong, L. (1973). Review of two-phase flow instability. *Nuclear Engineering and Design, 25*(2), 165-192.

[2] U.S. Nuclear Regulatory Commission. (1988). *Lasalle Unit 2 loss of recirculation pumps with power oscillation event* (Information Notice No. 89-33). Retrieved from https://www.nrc.gov/reading-rm/doc-collections/gen-comm/info-notices/1988/in88039.html

[3] U.S. Nuclear Regulatory Commission. (1992). *Power oscillations at Washington Nuclear Power Unit 2* (Information Notice No. 92-74). Retrieved from https://www.nrc.gov/reading-rm/doc-collections/gen-comm/info-notices/1992/in92074.html

[4] Wallis, G. B., & Heasley, J. H. (1961). Oscillations in two-phase flow systems. *Journal of Heat Transfer, 83*(3), 363-369.

[5] Ishii, M. (1971). *Thermally induced flow instabilities in two-phase mixtures in thermal equilibrium.* Georgia Institute of Technology.

[6] Saha, P., & Zuber, N. (1978). An analytical study of the thermally induced two-phase flow instabilities including the effect of thermal non-equilibrium. *International Journal of Heat and Mass Transfer, 21*(4), 415-426.

[7] Achard, J.-L., Drew, D. A., & Lahey, R. T. (1985). The analysis of nonlinear density-wave oscillations in boiling channels. *Journal of Fluid Mechanics, 155*, 213-232.

[8] Uddin, R. (1987). *Linear and nonlinear stability analyses of density-wave oscillations in heated channels.* (Doctoral dissertation), University of Illinois at Urbana-Champaign, Illinois, United States.

[9] Nayak, A. K., & Vijayan, P. K. (2008). Flow instabilities in boiling two-phase natural circulation systems: A review. *Science and Technology of Nuclear Installations, 2008*.

[10] Aritomi, M., Chiang, J. H., Nakahashi, T., Wataru, M., & Mori, M. (1992). Fundamental Study on Thermo-Hydraulics during Start-Up in Natural Circulation Boiling Water Reactors, (I). *Journal of Nuclear Science and Technology, 29*(7), 631-641.

[11] Furuya, M., Inada, F., & Yasuo, A. (1995). *Density wave oscillations of a boiling natural circulation loop induced by flashing.* Paper presented at the Proceedings of the 7th International Meeting on Nuclear Reactor Thermal-Hydraulics (NURETH-7), Saratoga Springs, NY.

[12] van der Hagen, T. H. J. J., & Stekelenburg, A. J. C. (1997). The low-power low-pressure flow resonance in a natural circulation cooled boiling water reactor. *Nuclear Engineering and Design, 177*(1), 229-238.

[13] Fukuda, K., & Kobori, T. (1979). Classification of two-phase flow instability by density wave oscillation model. *Journal of Nuclear Science and Technology, 16*(2), 95-108.

[14] Kim, J. M., & Lee, S. Y. (2000). Experimental observation of flow instability in a semi-closed two-phase natural circulation loop. *Nuclear Engineering and Design, 196*(3), 359-367.

[15] Manera, A., & van der Hagen, T. H. J. J. (2003). Stability of natural-circulation-cooled boiling water reactors during startup: Experimental results. *Nuclear Technology, 143*(1), 77-88.

[16] Marcel, C. P., Rohde, M., & Van Der Hagen, T. H. J. J. (2009). Experimental and numerical investigations on flashing-induced instabilities in a single channel. *Experimental Thermal and Fluid Science, 33*(8), 1197-1208.

[17] Dixit, A. (2010). *Stability of two-phase natural circulation reactor during start-up procedures.* (Doctoral Dissertation), Purdue University, West Lafayette, IN.

[18] Cloppenborg, T., Schuster, C., & Hurtado, A. (2015). Two-phase flow phenomena along an adiabatic riser – An experimental study at the test-facility GENEVA. *International Journal of Multiphase Flow, 72*, 112-132.

[19] Shi, S. (2015). *Investigation of natural circulation instability and transients in passively safe novel modular reactor.* (Doctoral Dissertation), Purdue University, West Lafayette, IN.

[20] Wang, Q., Gao, P., Chen, X., Wang, Z., & Huang, Y. (2018). An investigation on flashing-induced natural circulation instabilities based on RELAP5 code. *Annals of Nuclear Energy, 121*, 210-222.

[21] Furuya, M., Inada, F., & van der Hagen, T. H. J. J. (2005). Flashing-induced density wave oscillations in a natural circulation BWR—mechanism of instability and stability map. *Nuclear Engineering and Design, 235*(15), 1557-1569.

[22] Dixit, A., Hibiki, T., Ishii, M., Tanimoto, K., Kondoh, Y., & Hibi, K. (2013). Experimental stability maps for a two-phase natural circulation reactor with and without void-reactivity feedback effect. *Nuclear Engineering and Design, 261*, 181-200.

[23] Shi, S., Lin, Y.-C., Yang, W., & Ishii, M. (2015). *Experimental stability maps for a BWR-type small modular reactor.* Paper presented at the Proceedings of the 16th International Topical Meeting on Nuclear Reactor Thermal Hydraulics (NURETH-16), Chicago, IL.

[24] van der Hagen, T. H. J. J., van Bragt, D. D. B., van der Kaa, F. J., et al. (1997). Exploring the dodewaard type-I and type-II stability; from start-up to shut-down, from stable to unstable. *Annals of Nuclear Energy, 24*(8), 659-669.

[25] Dixit, A., Hibiki, T., Ishii, M., Tanimoto, K., Kondoh, Y., & Hibi, K. (2013). Start-up transient test simulation with and without void-reactivity feedback for a two-phase natural circulation reactor. *Nuclear Engineering and Design, 265*, 1131-1147.

[26] Shi, S., Schlegel, J. P., Brooks, C. S., et al. (2015). Experimental investigation of natural circulation instability in a BWR-type small modular reactor. *Progress in Nuclear Energy, 85*, 96-107.

[27] Jones, O. C., & Delhaye, J.-M. (1976). Transient and statistical measurement techniques for two-phase flows: A critical review. *International Journal of Multiphase Flow, 3*(2), 89-116.

[28] Shollenberger, K. A., Torczynski, J. R., Adkins, D. R., O'Hern, T. J., & Jackson, N. B. (1997). Gamma-densitometry tomography of gas holdup spatial distribution in industrial-scale bubble columns. *Chemical Engineering Science, 52*(13), 2037-2048.

[29] George, D. L., Torczynski, J. R., Shollenberger, K. A., O'Hern, T. J., & Ceccio, S. L. (2000). Validation of electrical-impedance tomography for measurements of material distribution in two-phase flows. *International Journal of Multiphase Flow, 26*(4), 549-581.

[30] Kim, S., Fu, X. Y., Wang, X., & Ishii, M. (2000). Development of the miniaturized four-sensor conductivity probe and the signal processing scheme. *International Journal of Heat and Mass Transfer, 43*(22), 4101-4118.

[31] Manera, A., Prasser, H. M., Lucas, D., & van der Hagen, T. H. J. J. (2006). Three-dimensional flow pattern visualization and bubble size distributions in stationary and transient upward flashing flow. *International Journal of Multiphase Flow, 32*(8), 996-1016.

[32] Prasser, H. M., Scholz, D., & Zippe, C. (2001). Bubble size measurement using wire-mesh sensors. *Flow Measurement and Instrumentation, 12*(4), 299-312.

[33] Ooi, Z. J., Kumar, V., & Brooks, C. S. (2019). Experimental database of two-phase natural circulation with local measurements. *Progress in Nuclear Energy, 116*, 124-136.

[34] Manera, A. (2003). *Experimental and analytical investigations on flashing-induced instabilities in natural circulation two-phase systems: Applications to the startup of boiling water reactors.* (Doctoral dissertation), Delft University of Technology, Delft, Netherlands.

[35] Ishii, M., & Hibiki, T. (2010). *Thermo-fluid dynamics of two-phase flow*: Springer Science & Business Media.

[36] Lee, S. Y., & Kim, Y. L. (1999). An analytical investigation of role of expansion tank in semi-closed two-phase natural circulation loop. *Nuclear Engineering and Design, 190*(3), 353-360.

[37] Inada, F., Furuya, M., & Yasuo, A. (2000). Thermo-hydraulic instability of boiling natural circulation loop induced by flashing (analytical consideration). *Nuclear Engineering and Design, 200*(1), 187-199.

[38] Shi, S., & Ishii, M. (2017). Modeling of flashing-induced flow instabilities for a natural circulation driven novel modular reactor. *Annals of Nuclear Energy, 101*, 215-225.

[39] Su, G., Jia, D., Fukuda, K., & Guo, Y. (2002). Theoretical and experimental study on density wave oscillation of two-phase natural circulation of low equilibrium quality. *Nuclear Engineering and Design, 215*(3), 187-198.

[40] Kim, S. (1999). *Interfacial area transport equation and measurement of local interfacial characteristics.* (Doctoral Dissertation), Purdue University, West Lafayette, IN.

[41] Fu, X. (2001). *Interfacial area measurement and transport modeling in air-water two-phase flow.* (Doctoral Dissertation), Purdue University, West Lafayette, IN.

[42] Worosz, T., Bernard, M., Kong, R., Toptan, A., Kim, S., & Hoxie, C. (2016). Sensitivity studies on the multi-sensor conductivity probe measurement technique for two-phase flows. *Nuclear Engineering and Design, 310*, 552-563.

APPENDIX A: UNCERTAINTY

A.1 General Procedure

For the current experiment, measurement is performed under transient conditions where most signals are intrinsically oscillating. Based on the periodicity widely reported in literature and also observed during the post-processing, the uncertainty analysis of the output data is performed with the assumed periodicity in the real dynamics of the natural circulation system.

The measurement covering multiple oscillation periods is thus equivalent to the repeating sampling, and the average operation over these periods, also known as the ensemble average, is performed as described in Section 2.3. For each instance t in the representative time, directly measured data points synchronized from n oscillation cycles are averaged to provide an estimation of the true value. The standard deviation $\sigma(t)$ of these data points provides a statistical way to estimate the uncertainty caused by the random error in the experiment. Noting the uncertainty caused systematic error as u_B corresponding to the maximum error, the overall uncertainty $u(t)$ of output data is combined as:

$$u(t) = \sqrt{{u_B}^2 + \left(3\frac{\sigma(t)}{\sqrt{n}}\right)^2}$$

which is a function of the representative time and also changes with conditions.

A.2 Instrumentational Uncertainty

The evaluation of systematic uncertainty u_B requires the knowledge of the error caused by the instrumentations. Table 3 summaries the corresponding information either provided by manufacturers, reported by other literature, or determined through experiments.

Table 3: Instrumentations and the associated measurement uncertainty

Parameter [Unit]	Instrumentation / Measurement Method	Maximum Instrumentational Uncertainty
System pressure [kPa]	① Rosemount™ 3051S Coplanar™ Pressure Transmitter Model: 3051S1CG4A2E11A1A Range: 0 ~ 1000 (kPa, gauge pressure) ② National Instruments™ NI 9203 current DAQ module	①0.025% of the span range = 0.25 kPa ②offset error = 0.02% range = 0.2 kPa gain error = 0.04% reading
Differential pressure [kPa]	① Rosemount™ 3051S Coplanar™ Pressure Transmitter Model: 3051S1CD4A2E11A1A Range: -60 ~ 60 (kPa, differential pressure) ② National Instruments™ NI 9203 current DAQ module	①0.025% of the span range = 0.03 kPa ②offset error = 0.02% range = 0.024 kPa gain error = 0.04% reading
Inlet volumetric velocity [m/s]	① Magnetic flow meter from Siemens™ Model: SITRANS F M MAG 5000 Range: -20 ~ 20 (gpm, volumetric flow rate) ② National Instruments™ NI 9203 current DAQ module	①if $\|v\| \geq 0.154$ m/s, 0.4% reading ± 0.00154 m/s if $\|v\| < 0.154$ m/s, 0.00384 m/s ②offset error = 0.02% range = 0.0003m/s gain error = 0.04% reading
Fluid temperature [℃]	① Ungrounded T-type thermocouple from OMEGA™ Model: TMQSS-062U-6 ② National Instruments™ NI 9212 / NI 9214 DAQ modules (internal cold junction compensation TB 9212 / TB9214)	①0.5 ℃ or 0.4% reading (greater one) ②0.33 ℃ under typical ambient temperature
Local void fraction [-]	① Customized four-sensor conductivity probes ② National Instruments™ NI 9222 / NI 9223 voltage DAQ modules	5% of the measured value, based on literature with similar four-sensor probe designs [33].
Heat flux [kW/m^2]	Determined by calibration tests	1.7% of the reported value
Inlet minor loss coefficient [-]	Determined by previous experiments	7% of the reported value

A.3 Overall Uncertainty

The overall uncertainty of the collected data is calculated using the procedure mentioned in Section A.1. The systematic uncertainty u_B is assumed to be dominated by the instrumentational error. The errors from instruments and DAQ modules are assumed to be independent so that their mean-square-root is used to combine them as u_B. A typical calculation result is shown in Fig. 16.

Measurement uncertainty is dominated by different contributing factors at different time and for different parameters. One commonly observed trend is that the uncertainty has relatively large values when the parameters experience steep changes. This trend is mainly dominated by the random error in the appearance time of these steep jumps, because small discrepancy in appearance time among different oscillation cycles can causes large discrepancy in the parameter values due to the large slopes. For simplicity, estimation using constant relative uncertainty can be used for the maximum uncertainty in flow rate and void fraction data which experience large jumps in the absolute values as shown in Fig. 16(b). For the fluid temperature data, the uncertainty is dominated by the instrumentational uncertainty, and a constant absolute uncertainty can properly represent the general maximum uncertainty. The uncertainty in the system pressure is dominated by the systematic error, while both instrumentational and random errors are important for the differential pressure between the inlet and instrumentation ports. Using a constant absolute uncertainty for all the pressure data can over-estimate the error in differential pressure data but is convenient in providing a conservative bound for the maximum uncertainty.

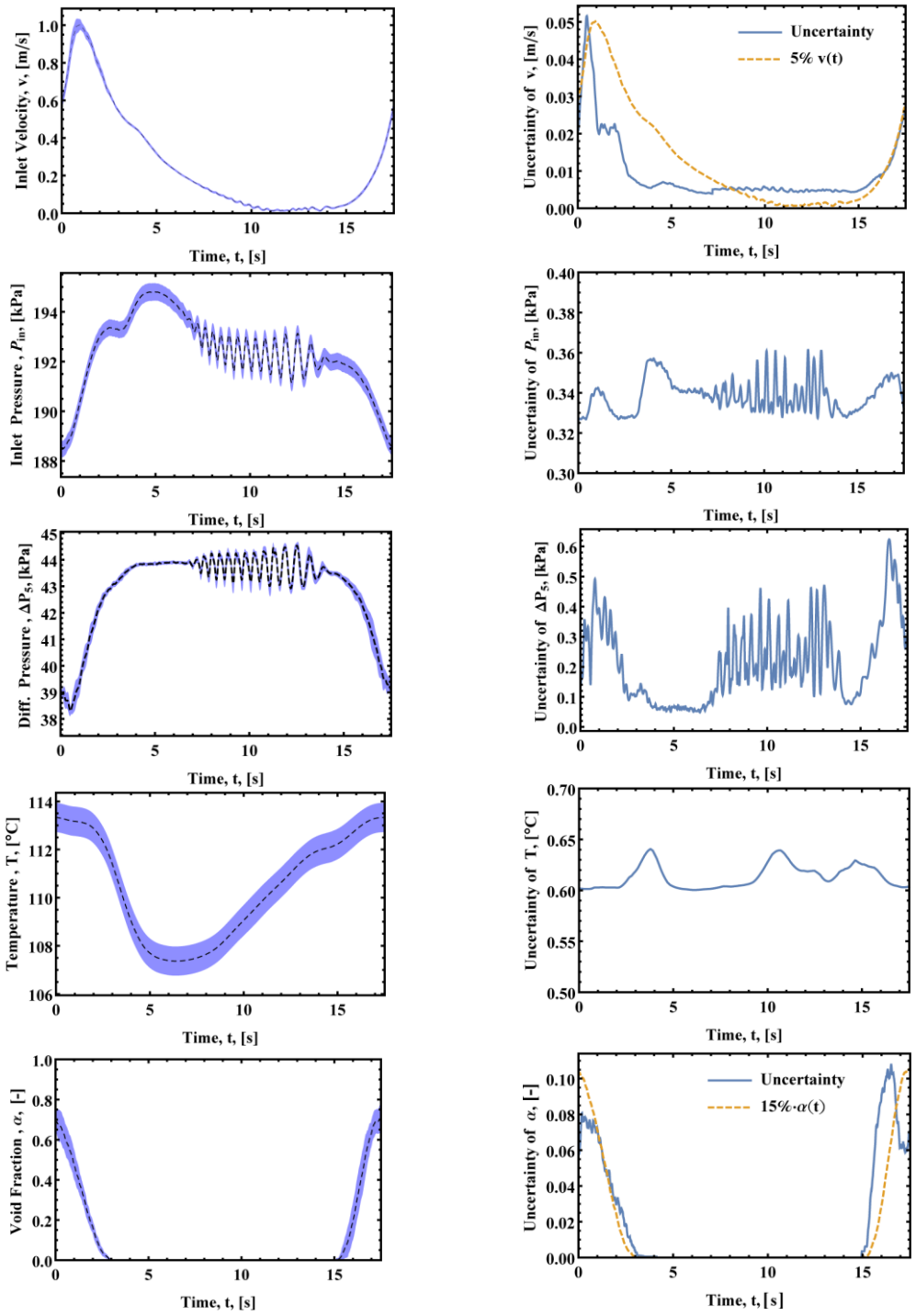

(a) (b)

Figure 16: Measurement uncertainty for an example condition. (P_{in} = 192kPa, $\Delta T_{sub,in}$ = 18.4°C, q = 45.4kW/m^2, K_{loss} = 22) (a) Parameters plotted with uncertainty regions. Blue regions function as the error bars. Temperature at Port 3 R^* = 0.5 and the void fraction at Port 4 R^* = 0.5 are plotted as examples. (b) Measurement uncertainty for the typical parameters plotted in (a).

Table 4 exhibits the general maximum uncertainty for all the periodic conditions collected in the current experiment. These values can overestimate the uncertainty for specific conditions and at specific time instants, so detailed maximum uncertainty as shown in Fig. 16 should be used if necessary.

Table 4: Maximum measurement uncertainty.

Parameters [Unit]	Maximum Uncertainty
System pressure [kPa]	0.4 kPa
Differential pressure [kPa]	0.6 kPa
Inlet volumetric velocity [m/s]	5% of the reported value or 0.03 m/s (greater one)
Fluid temperature [°C]	0.7 °C
Local void fraction [-]	15% of the reported value
Heat flux [kW/m^2]	1.7% of the reported value
Inlet minor loss coefficient [-]	7% of the reported value